Journal of Medicinal Chemistry

Article

Cite This: J. Med. Chem. 2019, 62, 11260−11279

pubs.acs.org/jmc

Synthesis of Peptoid-Based Class I-Selective Histone Deacetylase Inhibitors with Chemosensitizing Properties

Viktoria Krieger,[†,#] Alexandra Hamacher,[†,#] Fangyuan Cao,[⊥] Katharina Stenzel,[†] Christoph G. W. Gertzen,[†,¶,∥] Linda Schäker-Hübner,[§] Thomas Kurz,[†] Holger Gohlke,[†,∥] Frank J. Dekker,[⊥] Matthias U. Kassack,[*,†,‡] and Finn K. Hansen[*,§,‡]

[†]Institut für Pharmazeutische und Medizinische Chemie, Heinrich-Heine-Universität Düsseldorf, Universitätsstr. 1, 40225 Düsseldorf, Germany

[⊥]Department of Chemical and Pharmaceutical Biology, Groningen Research Institute of Pharmacy, University of Groningen, Antonius Deusinglaan 1, 9713 AV Groningen, The Netherlands

[∥]John von Neumann Institute for Computing (NIC), Jülich Supercomputing Centre (JSC), and Institute for Complex Systems - Structural Biochemistry (ICS-6), Forschungszentrum Jülich GmbH, Wilhelm-Johnen-Straße, 52425 Jülich, Germany

[¶]Center for Structural Studies (CSS), Heinrich-Heine-Universität Düsseldorf, Universitätsstr. 1, 40225 Düsseldorf, Germany

[§]Pharmaceutical/Medicinal Chemistry, Institute of Pharmacy, Medical Faculty, Leipzig University, Brüderstraße 34, 04103 Leipzig, Germany

S *Supporting Information*

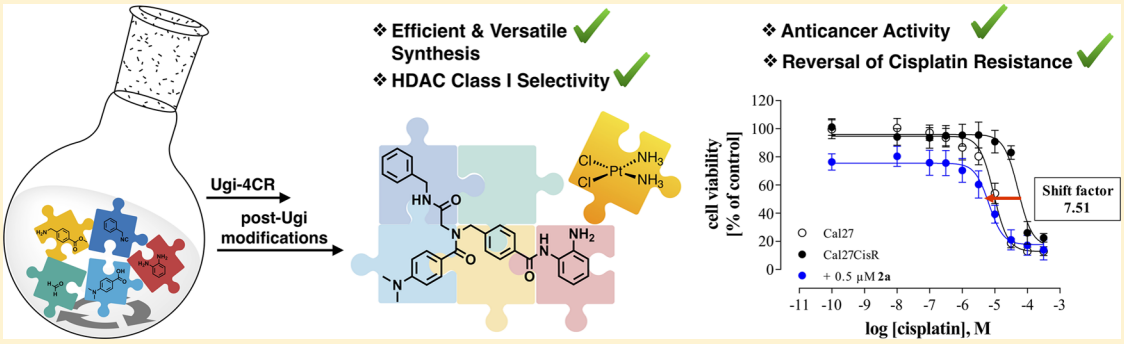

ABSTRACT: There is increasing evidence that histone deacetylase (HDAC) inhibitors can (re)sensitize cancer cells for chemotherapeutics via "epigenetic priming". In this work, we describe the synthesis of a series of class I-selective HDAC inhibitors with 2-aminoanilides as zinc-binding groups. Several of the synthesized compounds revealed potent inhibition of the class I HDAC isoforms HDAC1, HDAC2, and/or HDAC3 and promising antiproliferative effects in the human ovarian cancer cell line A2780 and the human squamous carcinoma cell line Cal27. Selected compounds were investigated in a cellular model of platinum resistance. In particular, compound **2a** revealed potent chemosensitizing properties and full reversal of cisplatin resistance in Cal27CisR cells. This effect is related to a synergistic increase in caspase 3/7 activation and induction of apoptosis. Thus, this work demonstrates that pan-HDAC inhibition or dual class I/class IIb inhibition is not required for full reversal of cisplatin resistance.

INTRODUCTION

Diverse cellular functions are regulated by dynamic modifications, metabolism, transcription, and translation.[1] The acetylation and deacetylation of lysine belongs to crucial post-translational modifications in the epigenetic field. Epigenetics deals with heritable changes in gene expression without influence of the DNA sequence itself.[1] One way to alter gene expression is the histone acetylation status, which is controlled via histone acetyl transferases (HATs) and histone deacetylases (HDACs). HDAC proteins are responsible for the deacetylation of lysine residues located on the amino-terminal tails of histone proteins. The deacetylation induces condensed and transcriptionally inactive heterochromatin. Interference with the acetylation/deacetylation process has been linked to cancer development. Inhibition of HDACs, which are overexpressed in several cancer types, results in the expression of genes leading to terminal differentiation, growth arrest, and/or apoptosis in cancer cells.[2] Thus, the inhibition of HDACs has become an important target in cancer research. To date, four HDAC inhibitors (HDACi's) have received FDA-approval in cancer treatment. The first three approvals for HDACi's (vorinostat, romidepsin, and belinostat; Figure 1) have been granted for the treatment of rare types of lymphoma

Received: September 7, 2019
Published: November 24, 2019

DOI: 10.1021/acs.jmedchem.9b01489
J. Med. Chem. 2019, 62, 11260−11279

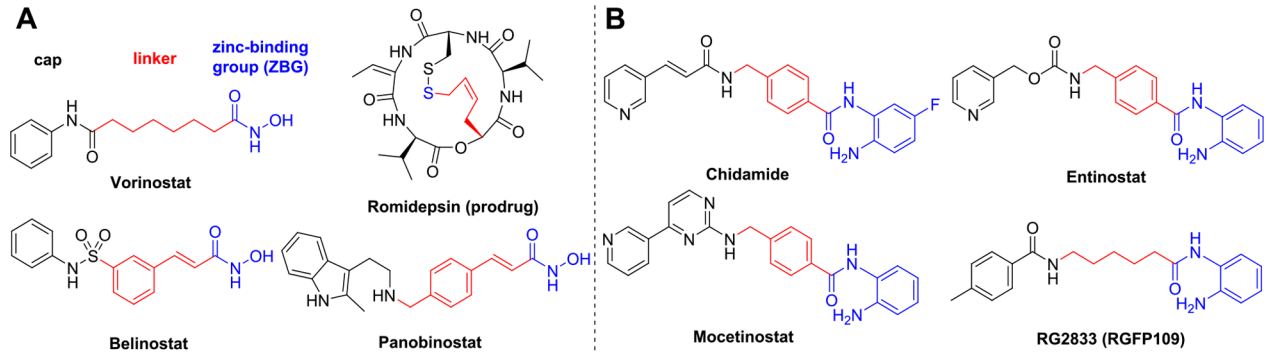

Figure 1. FDA-approved (A) HDACi's and (B) aminoanilide-based HDACi's.

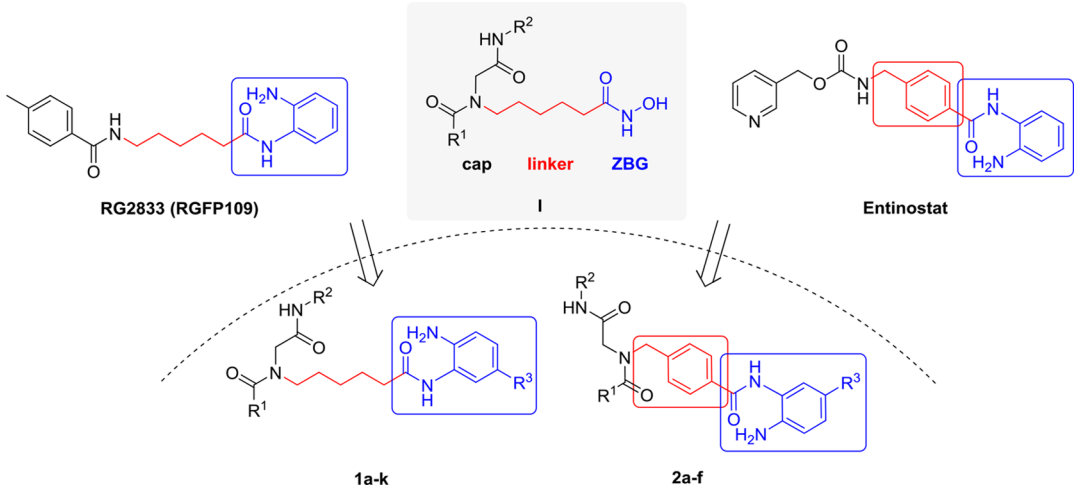

Figure 2. Design of target compounds **1a–k** and **2a–f**.

(cutaneous T-cell lymphoma (CTCL) and/or peripheral T-cell lymphoma (PTCL)). However, the approval of panobinostat (Figure 1) to treat multiple myeloma is good evidence for the application of HDACi's in more common cancer types.[3] Beyond hematologic cancers, HDACi's have reached advanced stages of clinical studies in solid cancers.[3] Furthermore, HDACi's have shown therapeutic potential in several other diseases beyond cancer such as parasitic diseases, immune disorders, HIV, inflammation, and neurodegenerative diseases.[4]

In humans, 18 different HDAC isoforms have been described and classified into four classes based on their homology to yeast HDACs. Class I (HDAC1, 2, 3, 8), class IIa (HDAC4, 5, 7, 9), class IIb (HDAC6, 10), and class IV (HDAC11) HDACs are Zn^{2+}-dependent enzymes, whereas class III HDACs are NAD^{+}-dependent (sirtuins).[5] The aforementioned hydroxamate-based HDACi's (vorinostat, belinostat, and panobinostat) do not exert selectivity toward a specific isoform. In addition, the potential genotoxicity of hydroxamate-containing HDACi's represents a major drawback in their application and has fueled the search for alternative ZBGs.[6] In this regard, 2-aminoanilides have emerged as promising alternatives to hydroxamates. Notably, they possess a different isoform profile compared to most hydroxamates and do not exhibit genotoxicity.[3,6] In detail, 2-aminoanilides display selectivity for HDAC1, HDAC2, and HDAC3, which can be further fine-tuned toward HDAC1 and HDAC2 by the introduction of bulky (hetero)aromatic substituents in the 5-position of the 2-aminoanilide scaffold. In the latter case, the additional (hetero)aromatic group is binding to a hydrophobic 14 Å cavity (the so-called "foot pocket")[7] in HDAC1 and HDAC2.

There is increasing evidence that 2-aminoanilides can succeed in clinical trials. For instance, chidamide (tucidinostat, Figure 1B) has been approved in China for relapsed or refractory PTCL.[8] Furthermore, entinostat (MS-275, phase III, Figure 1B), mocetinostat (MGCD0103, phase II, Figure 1B), and RG2833 (RGFP109, phase I, Figure 1B) show selective inhibition of class I HDACs and are currently studied in different stages of clinical trials.[3,9] Interestingly, RG2833 is developed as a drug against the neurodegenerative disease Friedreich ataxia (FRDA), which highlights the therapeutic potential of aminoanilide-based HDACi's beyond oncology.[9]

We previously discovered hydroxamate-based HDACi's utilizing peptoid-based cap groups, which are accessible by a facile synthetic protocol based on the Ugi four-component reaction (U-4CR).[10,11] Peptoid-based hydroxamates with a benzyl linker were identified as HDAC6 preferential inhibitors,[10] whereas hydroxamic acids with an alkyl linker displayed a preference for class I isoforms.[11] Several peptoid-based hydroxamates showed promising chemosensitizing properties and were able to revert cisplatin resistance in cancer cells.[10,11] Due to the aforementioned drawbacks of hydroxamic acids, we aimed at the development of peptoid-based HDACi's with a 2-aminoanilide ZBG. We herein report on the rational design, diversity-oriented synthesis, and biological evaluation of class I-selective HDACi's with peptoid-based cap groups.

DOI: 10.1021/acs.jmedchem.9b01489
J. Med. Chem. 2019, 62, 11260−11279

Scheme 1. Synthesis of Benzamide HDACi's 1a−h[a]

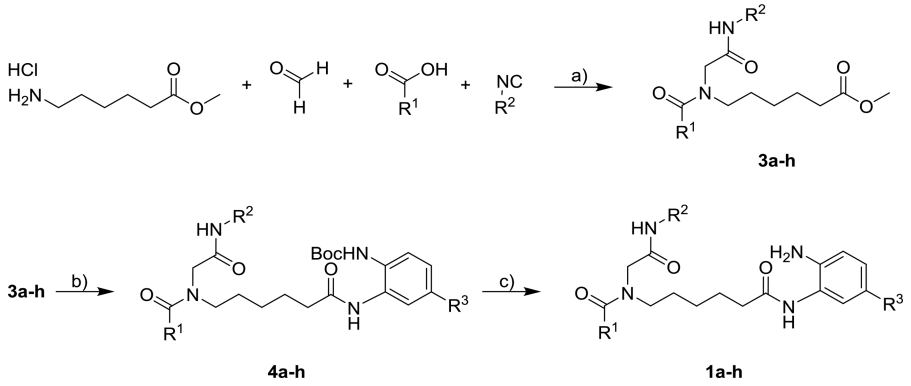

[a]Reagents and conditions: (a) (i) methyl 6-aminohexanoate hydrochloride (1.2 equiv), paraformaldehyde (1.2 equiv), MeOH, 4 Å MS, RT, 30 min; (ii) R^1COOH (1 equiv), RT, 10 min; (iii) R^2NC (1 equiv), RT, 16 h; (b) (i) LiOH·H_2O (2 equiv), MeOH, RT, 16 h; (ii) acid (1.2 equiv), amine (1 equiv), pyridine (2 equiv), DIC (1.2 equiv), HOAt (1.2 equiv), CH_2Cl_2/DMF (1:1, v/v), RT, 16 h; (c) TFA/CH_2Cl_2 (1:5, v/v), RT, 30 min.

Scheme 2. Submonomer Synthesis of Compound 1i[a]

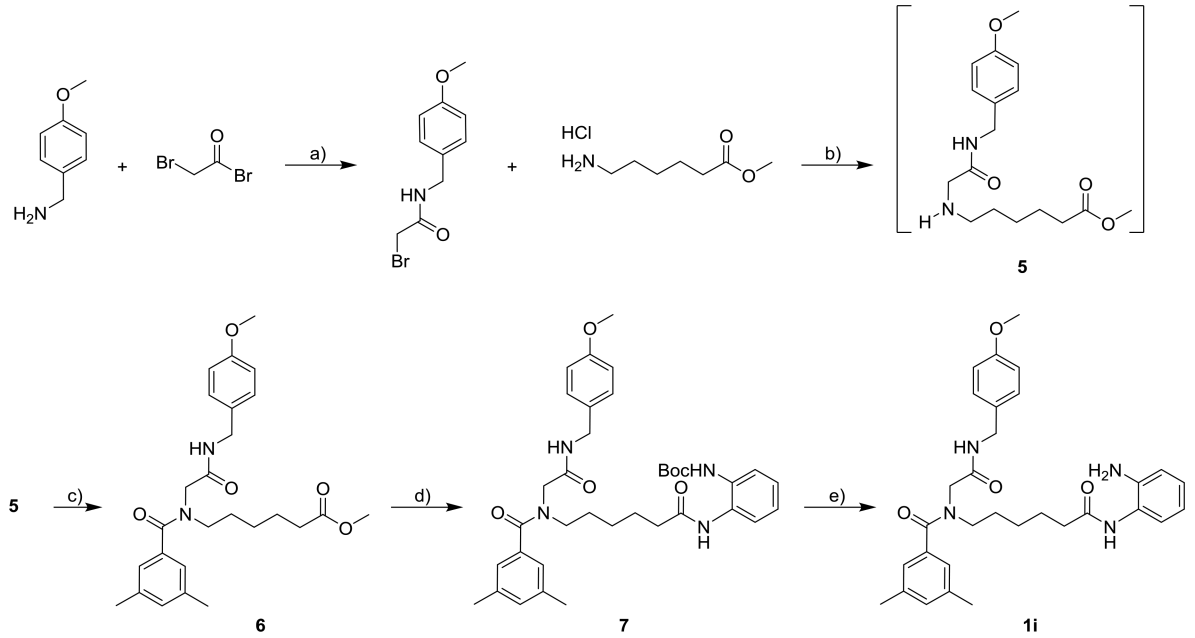

[a]Reagents and conditions: (a) (4-methoxyphenyl)methanamine (1 equiv), 2-bromoacetyl bromide (1 equiv), DIPEA (1 equiv), CH_2Cl_2, 0 °C → RT, 16 h; (b) methyl 6-aminohexanoate hydrochloride (1 equiv), 2-bromo-*N*-(4-methoxybenzyl)acetamide (1 equiv), Et_3N (2 equiv), CH_2Cl_2, RT, 16 h; (c) methyl 6-({2-[(4-methoxybenzyl)amino]-2-oxoethyl}amino)hexanoate (1.2 equiv), pyridine (1.2 equiv), 3,5-dimethylbenzoyl chloride (1 equiv), CH_2Cl_2, 0 °C → RT, 16 h; (d) (i) LiOH·H_2O (2 equiv), MeOH, RT, 16 h; (ii) acid (1.2 equiv), *tert*-butyl-(2-aminophenyl)carbamate (1 equiv), pyridine (2 equiv), DIC (1.2 equiv), HOAt (1.2 equiv), CH_2Cl_2/DMF (1:1, v/v), RT, 24 h; (e) TFA/CH_2Cl_2 (15%, v/v), RT, 30 min.

RESULTS AND DISCUSSION

Design and Synthesis of Peptoid-Based 2-Aminoanilides. The synthesis of our HDACi library is summarized in Schemes 1−3. The series HDACi's **1a−k** were designed as hybrid compounds derived from our peptoid-based hydroxamate scaffold **I** and RG2833 (Figure 2). We retained the aliphatic linker and substituted the hydroxamate-based ZBG by an aminoanilide-based ZBG in order to improve the selectivity for the class I isoforms HDAC1−HDAC3. The synthesis of compounds **1a−h** was achieved through straightforward U-4CRs differing in the use of the carboxylic acid and the isocyanide components (Scheme 1). In detail, for the synthesis of compounds **3a−h**, the amine methyl 6-aminohexanoate hydrochloride, trimethylamine, and paraformaldehyde were stirred in dry methanol in the presence of 4 Å molecular sieves (4 Å MSs) to provide the imine intermediate. The subsequent addition of the carboxylic acid and isocyanide component provided the desired Ugi products **3a−h** after purification by flash column chromatography (Scheme 1).

The target compounds **1a−h** were subsequently prepared by performing suitable post-Ugi transformations. The methyl esters of **3a−h** were cleaved via hydrolysis with LiOH·H_2O in methanol overnight. Afterward, the resulting carboxylic acids were coupled with the respective mono-Boc-protected phenylenediamine derivative using the coupling reagents DIC and HOAt in the presence of pyridine in CH_2Cl_2/DMF to afford

DOI: 10.1021/acs.jmedchem.9b01489
J. Med. Chem. 2019, 62, 11260−11279

Scheme 3. Submonomer Synthesis of Compounds 1j,k[a]

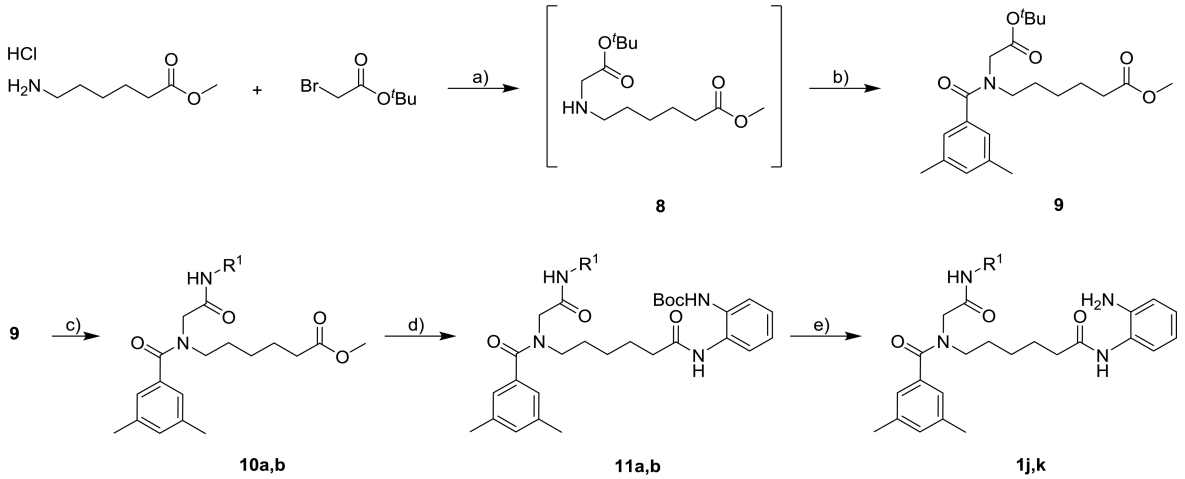

[a]Reagents and conditions: (a) methyl 6-aminohexanoate hydrochloride (1 equiv), *tert*-butylbromoacetate (1 equiv), Et_3N (2 equiv), THF, RT, 16 h; (b) methyl 6-{[2-(*tert*-butoxy)-2-oxoethyl]-amino}hexanoate (1.2 equiv), pyridine (1.2 equiv), 3,5-dimethylbenzoyl chloride (1 equiv), CH_2Cl_2, RT, 18 h; (c) (i) TFA/CH_2Cl_2 (1:5, v/v), RT, 2 h; (ii) acid (1 equiv), amine (1 equiv), EDC·HCl (2 equiv), DMAP (0.4 equiv), DMF/CH_2Cl_2, RT, 16 h; (d) (i) LiOH·H_2O (2 equiv), MeOH, RT, 16 h; (ii) acid (1.2 equiv), *tert*-butyl-(2-aminophenyl)carbamate (1 equiv), pyridine (2 equiv), DIC (1.2 equiv), HOAt (1.2 equiv), CH_2Cl_2/DMF (1:1, v/v), RT, 24 h; (e) TFA/CH_2Cl_2 (15%, v/v), RT, 30 min.

Scheme 4. Synthesis of HDACi's 2a–f[a]

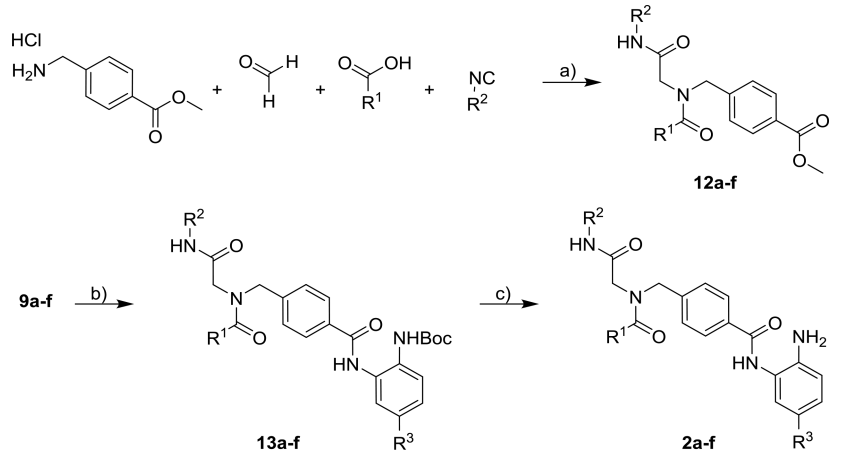

[a]Reagents and conditions: (a) (i) methyl 4-(aminomethyl)benzoate hydrochloride (1.2 equiv), paraformaldehyde (1.2 equiv), MeOH, 4 Å MS, RT, 30 min; (ii) R^1COOH (1 equiv), RT, 10 min; (iii) R^2NC (1 equiv), RT, 16 h; (b) (i) LiOH·H_2O (2 equiv), MeOH, RT, 16 h; (ii) acid (1.2 equiv), amine (1 equiv), EDC·HCl (2 equiv), DMAP (0.4 equiv), RT, 16 h; (c) TFA/CH_2Cl_2 (1:5, v/v), RT, 30 min.

the Boc-protected compounds **4a–h**. Finally, the acidic deprotection yielded the desired peptoid-based HDACi's **1a–h**.

Since the number of purchasable isocyanides is limited, we switched to a peptoid submonomer synthesis for further modifications of the isocyanide region (Schemes 2 and 3). The synthesis of compound **1i** is illustrated in Scheme 2. The reaction of 4-methoxybenzylamine with bromoacetyl bromide in the presence of DIPEA afforded the corresponding bromoacetyl amide. The subsequent alkylation of methyl 6-aminohexanoate hydrochloride in the presence of triethylamine in dichloromethane yielded the secondary amine **5**. Intermediate **5** was directly treated with 3,5-dimethylbenzoyl chloride using pyridine as a base to generate the peptoid **6**. The methyl ester in **6** was hydrolyzed, and the resulting carboxylic acid derivative was subjected to an amide coupling reaction with mono-Boc-protected phenylenediamine to yield **7**. Removal of the Boc-protecting group furnished the desired aminoanilide **1i**.

The synthesis of HDACi's **1j,k** was performed as highlighted in Scheme 3. The alkylation of methyl 6-aminohexanoate hydrochloride with *tert*-butyl bromoacetate in the presence of triethylamine in THF provided the secondary amine **8**. Without further purification, the intermediate **8** was directly acylated with 3,5-dimethylbenzoyl chloride using pyridine as a base to furnish the key building block **9**. Subsequently, **9** was used as a starting point for the variation of the isocyanide region. To this end, we performed the deprotection of the *tert*-butyl group followed by amide coupling reactions of the free carboxylic acid with the respective amine using DIC and HOAt as coupling agents to furnish **10a,b**. HDACi's **1j,k** were prepared via the saponification of the methyl ester in **10a,b** and a subsequent amide coupling with *tert*-butyl-(2-aminophenyl)-carbamate to yield **11a,b**. Next, the Boc-protecting group was removed by acidolysis to afford the target compounds **1j,k**.

DOI: 10.1021/acs.jmedchem.9b01489
J. Med. Chem. 2019, 62, 11260–11279

Table 1. Inhibitory Activities (IC_{50} [μM]) of Compounds 1a−k and 2a−f against HDAC1−HDAC3 and HDAC6

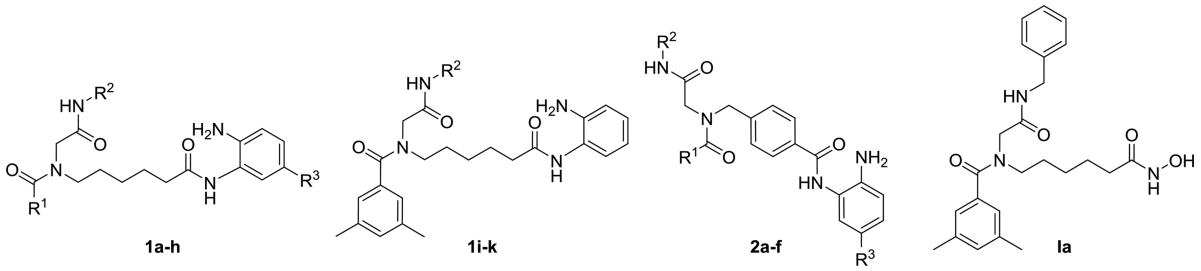

				IC_{50} [μM]			
compd	R^1	R^2	R^3	HDAC1	HDAC2	HDAC3	HDAC6
1a	Ph	c-Hex	H	5.46 ± 0.32	5.95 ± 0.67	0.858 ± 0.066	>10[a]
1b	3,5-Me-Ph	c-Hex	H	5.55 ± 0.30	6.66 ± 0.44	0.481 ± 0.088	>10[a]
1c	4-Me_2N-Ph	Bn	H	1.58 ± 0.15	1.24 ± 0.078	0.312 ± 0.021	>10[a]
1d	3,5-Me-Ph	Bn	H	1.16 ± 0.21	1.60 ± 0.38	0.250 ± 0.021	>10[a]
1e	1-naphthyl	c-Hex	H	6.56 ± 0.84	5.38 ± 0.69	0.646 ± 0.066	>10[a]
1f	1-naphthyl	Bn	H	1.67 ± 0.17	1.90 ± 0.030	0.163 ± 0.013	>10[a]
1g	4-Me_2N-Ph	Bn	F	1.98 ± 0.028	3.06 ± 0.16	0.369 ± 0.009	>10[a]
1h	3,5-Me-Ph	Bn	Ph	0.057 ± 0.005	1.81 ± 0.12	20% at 10 μM[b]	>10[a]
1i	3,5-Me-Ph	4-MeO-Bn	H	2.08 ± 0.21	30% at 10 μM[b]	49% at 10 μM[b]	>10[a]
1j	3,5-Me-Ph	4-Me-Bn	H	1.10 ± 0.05	5.03 ± 0.69	0.478 ± 0.026	>10[a]
1k	3,5-Me-Ph	3,5-Me-Bn	H	0.484 ± 0.051	4.10 ± 0.29	0.583 ± 0.027	>10[a]
2a	4-Me_2N-Ph	Bn	H	0.038 ± 0.012	0.283 ± 0.028	0.586 ± 0.055	>10[a]
2b	3,5-Me-Ph	Bn	H	0.062 ± 0.012	0.485 ± 0.018	32% at 10 μM[b]	>10[a]
2c	3-pyridyl	Bn	H	0.103 ± 0.016	0.786 ± 0.017	0.878 ± 0.117	>10[a]
2d	3,5-Me-Ph	Bn	Ph	0.051 ± 0.011	34% at 3.33 μM[b]	>10000[a]	>10[a]
2e	4-Me_2N-Ph	Bn	Ph	0.039 ± 0.011	36% at 3.33 μM[b]	>10000[a]	>10[a]
2f	3,5-Me-Ph	Bn	F	0.277 ± 0.045	25% at 10 μM[b]	23% at 10 μM[b]	>10[a]
vorinostat				0.111 ± 0.015	0.146 ± 0.014	0.0097 ± 0.0008	0.102 ± 0.009
entinostat				0.519 ± 0.063	0.505 ± 0.028	2.85 ± 0.22	>10[a]
RG2833				K_i = 0.032[c]	n.d.	K_i = 0.005[c]	n.d.
Ia	3,5-Me-Ph	Bn		0.025 ± 0.007[d]	0.061 ± 0.003[d]	0.026 ± 0.002[d]	0.135 ± 0.013[d]

[a]<15% inhibition at 10 μM. [b]% inhibition at the concentration stated (μM). [c]Data taken from ref 9b. [d]Data taken from ref 11.

The second type of HDACi's **2a−f** (Figure 2) is derived from our peptoid-based hydroxamate scaffold **I** and entinostat (MS-275), a selective inhibitor of HDAC1, HDAC2, and HDAC3. Compared to the first type of HDACi **1a−k**, they differ in their linker. The synthesis of compounds **2a−f** was performed essentially as described for compounds **1a−h** (Scheme 4). Briefly, in the case of compounds **2a−f**, we used methyl 4-(aminomethyl)benzoate as the amine component in the U-4CR to provide the intermediates **12a−f** bearing a benzyl linker. The Boc-protected aminoanilides **13a−f** were then prepared by hydrolysis of the methyl ester followed by amide coupling reactions with the respective mono-Boc-protected phenylenediamine derivative. Finally, deprotection of the Boc group was achieved by treatment of **13a−f** with trifluoroacetic acid in dichloromethane to provide the peptoid-based HDACi's **2a−f**.

Inhibition of HDAC1−HDAC3 and HDAC6. All synthesized compounds and the reference HDACi vorinostat were first screened for inhibitory activity against their intended targets HDAC1−HDAC3. Furthermore, HDAC6 was selected as the control isoform. The results are summarized in Table 1. As expected, all aminoanilides were inactive against HDAC6 (IC_{50} > 10 μM). The screening against HDAC1−HDAC3 provided some interesting differences depending on the type of linker and ZBG. In general, the 2-aminoanilides with a benzyl linker exhibited increased activity against HDAC1 and HDAC2 compared to their corresponding alkyl linker counterparts, whereas the alkyl-based compounds showed higher activity against HDAC3 (see for example **1c** vs **2a**). Compound **1h** bearing a phenyl ring in the R^3 position, which is intended to target the foot pocket in HDAC1 and HDAC2, represents one noteworthy exemption. **1h** revealed clearly the highest activity against HDAC1 (IC_{50}: 0.057 μM) among the alkyl-based compounds and is almost inactive against HDAC3 (20% inhibition at 10 μM). Interestingly, compound **1d** utilizes the same cap and linker as compound **1h** and the only difference in the structure is the additional phenyl ring at the R^3 position. The introduction of this foot pocket targeting moiety leads to an ∼20-fold improved potency of **1h** toward HDAC1 and a >40-fold reduction in activity against HDAC3 compared to **1d**. The hydroxamic acid-based HDACi **Ia** (Table 1), one of the hit compounds from our previous study,[11] represents the corresponding hydroxamate analogue of **1d** and **1h**. This compound showed potent inhibition of HDAC1−HDAC3 and HDAC6 with IC_{50} values ranging from 0.025 to 0.135 μM. Interestingly, the HDAC selectivity profile of this compound can be altered toward HDAC3 preferential inhibition by replacing the hydroxamate with an unsubstituted aminoanilide or toward HDAC1 preferential inhibition via the introduction of a foot pocket targeting moiety.

In the case of the benzyl-based compounds, no noteworthy change in potency against HDAC1 was observed after

DOI: 10.1021/acs.jmedchem.9b01489
J. Med. Chem. 2019, 62, 11260−11279

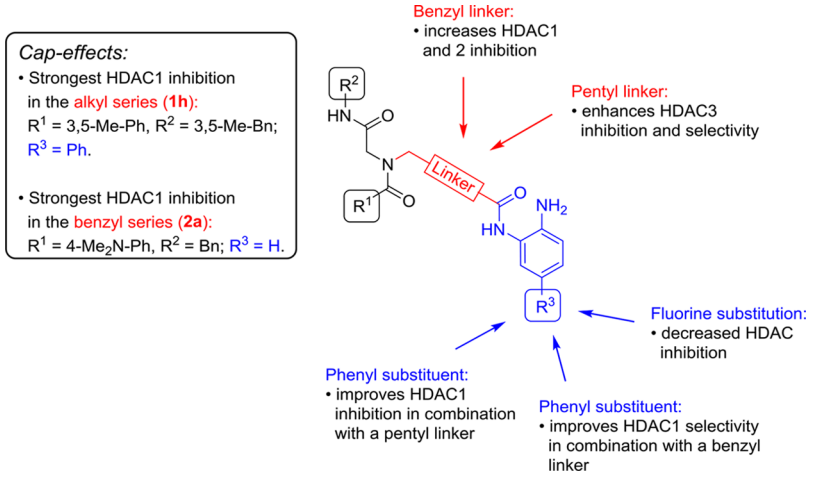

Figure 3. Structure–activity and structure–selectivity relationships of the peptoid-based aminoanilides **1a–k** and **2a–f**.

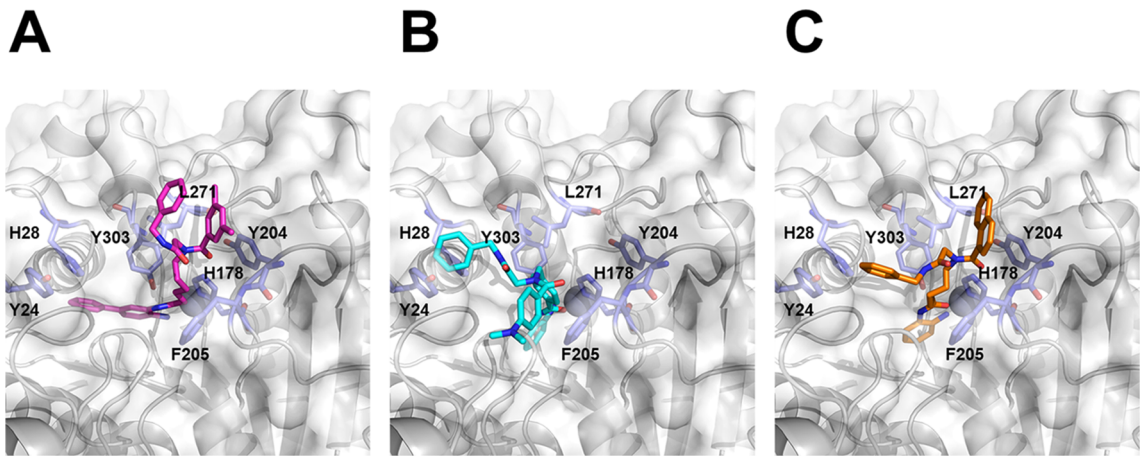

Figure 4. Predicted binding modes of compounds (A) *cis*-**1h** (magenta), (B) *cis*-**2a** (light blue), and (C) *cis*-**1f** (orange) in the energetically relaxed X-ray crystal structure of HDAC1 (white, cartoon, and surface, PDB ID 4BKX). Prominent interacting residues of HDAC1 are shown in navy sticks. (A) Compound *cis*-**1h** utilizes its spacious ZBG to fill the hydrophobic foot pocket in HDAC1 and engages in π-stacking interactions with Y204. (B) Compound *cis*-**2a** engages in π-stacking interactions with H28 and F205. (C) Compound *cis*-**1f** engages in π-stacking interactions with H28 and Y204.

introduction of an additional phenyl ring at the aminoanilide group (see **2a** (IC_{50}: 0.038 μM) vs **2e** (IC_{50}: 0.039 μM)). As expected, compound **2e** was inactive against HDAC3. Notably, the introduction of a fluorine atom in the R^3 position, as realized in the approved aminoanilide chidamide, resulted in a significant decrease of the HDAC1 and HDAC2 inhibition (see **2b** vs **2f**) and hence this substitution appears to be detrimental to our peptoid-based aminoanilides. Compared to the well-known aminoanilide entinostat (HDAC1 IC_{50}: 0.519 μM; HDAC2 IC_{50}: 0.505 μM; and HDAC3 IC_{50}: 2.85 μM,), our benzyl-based compounds **2a–f** displayed an improved inhibition of HDAC1 and a clear preference for HDAC1 over HDAC2 and HDAC3 (Table 1).

Interestingly, compounds **1h** (alkyl linker) and **2d** (benzyl linker) bearing the same cap and ZBG revealed similar inhibition profiles with potent inhibition of HDAC1 (**1h** (IC_{50}: 0.057 μM) vs **2d** (IC_{50}: 0.051 μM)) and weak inhibition of HDAC2 and HDAC3. In contrast, compounds **1c** and **2a**, which also only differ in the linker, showed a completely different inhibition profile with **1c** being an HDAC3 preferential inhibitor, whereas **2a** displayed HDAC1 preference. Based on these results, it can be assumed that, in the absence of a foot pocket group, the linker dictates the selectivity profile. However, as soon as a foot pocket-targeting moiety is added to the aminoanilide ZBG, the ability of the substituted aminoanilide ZBG to occupy the foot pocket is responsible for the preferential inhibition of HDAC1.

The most important structure–activity and structure–selectivity relationships are summarized in Figure 3. Overall, this screening revealed the alkyl-based compound **1f** as the most potent preferential HDAC3 inhibitor and the benzyl-based compounds **2d,e** as preferential HDAC1 inhibitors. Furthermore, **1h** and **2a** were identified as the most potent HDAC1 inhibitors from the alkyl and benzyl series, respectively.

Docking Studies. Compounds **1h** and **2a**, which showed the highest activity against HDAC1 within each molecule series, respectively, and **1f**, which showed preferential inhibition of HDAC3, were docked into energetically relaxed X-ray crystal structures of HDAC1, HDAC2, HDAC3, and HDAC6. We docked the three compounds in both their *cis*- and *trans*-rotamers, considering the orientation of the amide bond connecting R^1. While valid docking poses of all three compounds were identified in HDAC1 and HDAC2,

DOI: 10.1021/acs.jmedchem.9b01489
J. Med. Chem. 2019, 62, 11260–11279

Table 2. Cytotoxic Activity of Compounds 1a−k and 2a−f[a]

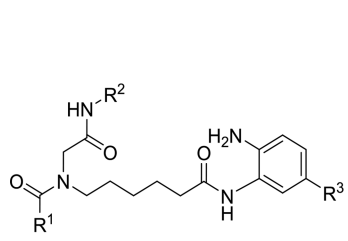

1a-h

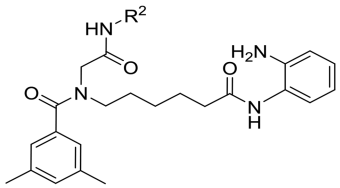

1i-k

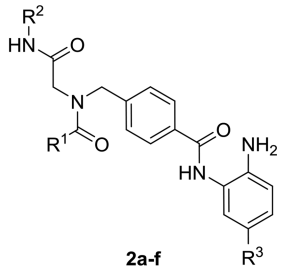

2a-f

compd	R^1	R^2	R^3	MTT IC_{50} [μM] A2780	MTT IC_{50} [μM] Cal27
1a	Ph	c-Hex	H	181	30.9
1b	3,5-Me-Ph	c-Hex	H	42.0	17.5
1c	4-Me_2N-Ph	Bn	H	18.5	16.0
1d	3,5-Me-Ph	Bn	H	20.9	13.7
1e	1-naphthyl	c-Hex	H	18.1	24.9
1f	1-naphthyl	Bn	H	22.8	11.0
1g	4-Me_2N-Ph	Bn	F	25.9	20.2
1h	3,5-Me-Ph	Bn	Ph	17.1	18.9
1i	3,5-Me-Ph	4-MeO-Bn	H	24.6	17.4
1j	3,5-Me-Ph	4-Me-Bn	H	9.80	18.2
1k	3,5-Me-Ph	3,5-Me-Bn	H	5.10	19.3
2a	4-Me_2N-Ph	Bn	H	2.40	1.60
2b	3,5-Me-Ph	Bn	H	2.80	1.60
2c	3-Pyridyl	Bn	H	8.90	11.2
2d	3,5-Me-Ph	Bn	Ph	n.e.	8.90
2e	4-Me_2N-Ph	Bn	Ph	n.e.	11.1
2f	3,5-Me-Ph	Bn	F	5.40	5.72
vorinostat				2.42	2.64
cisplatin				2.25	2.50

[a]Values are the mean of three experiments. Standard deviations are <10% of the mean. n.e. = no effect up to 100 μM.

molecular docking failed in the case of HDAC6: Here, no docking pose could be identified in which the ZBG of the respective compound was interacting with the Zn^{2+} ion at the catalytic center of HDAC6 (Table S1). The reason for this is the shape of the catalytic center in HDAC6, which is too narrow to accommodate the sterically demanding ZBG of the compounds. As the interaction of the ZBG with the zinc ion is known to be essential for the activity of HDACi's, these results are in perfect agreement with the compounds' inability to inhibit HDAC6 (Table 1). Both **1f** and **2a** furthermore produce valid docking poses in HDAC3 (Table 1). Thus, the docking results neither replicate the HDAC3 preference of **1f** nor the HDAC1 preference of **2a**; however, given the small differences in the respective IC_{50} values (Table 1), such a discrimination cannot be expected from a scoring function.[12] Yet, the docking results do reflect the compounds' general ability to inhibit the three HDAC isoforms (Table 1). The validity of the docking is further corroborated by the results of compound **1h**, for which valid docking poses were obtained in HDAC1 and HDAC2 but not in HDAC3 (Table S1), in line with inhibition studies (Table 1).

Judging from the docking results of the three HDACi's, the binding affinity to HDAC1 seems to be dominated by the aromatic character and size of the ZBG and linker. As such, **1h** and **2a**, which show a high affinity toward HDAC1, bear an additional phenyl ring in their structure: In **1h**, the phenyl ring is in position R^3 with which it occupies the foot pocket adjacent to the zinc ion of HDAC1 (Figure 4A); in **2a**, the phenyl ring is in the linker forming π-stacking interactions to H178 (Figure 4B). In contrast, **1f**, which shows a lower affinity toward HDAC1 than the other two compounds, bears neither of the two aforementioned features. For the substituents in R^1 and R^2, no common interaction pattern can be found for all three tested HDACi's. While **1f** and **1h** both interact with Y204, **1h** forms hydrophobic contacts with L271, and **1f** forms π-stacking interactions with H28 (Figure 4A,C). H28 is also addressed by π-stacking interactions by **2a**, yet R^1 of this compound forms π-stacking interactions with F205. The inability of **1h** to inhibit HDAC3 is caused by a spacious phenyl ring in R^3, which does not fit the binding pocket of HDAC3. As the residues lining the binding pocket of HDAC1 and HDAC2 are highly identical (96%, considering residues 8 Å around the co-crystallized ligand of the HDAC2 complex structure as part of the binding pocket), similar docking results for both isoforms could be expected. However, the energetic relaxation of the two structures widened the brim of the HDAC2 binding pocket by ∼1 Å more than that of HDAC1, which allows HDAC2 to also accommodate the more spacious *trans*-rotamers of the HDACi.

To conclude, while the docking cannot reproduce subtle selectivity differences, it is able to correctly predict and rationalize the ligands' general capabilities to inhibit the HDAC isoforms 1, 2, and 3.

Anticancer Activity and Inhibition of Cellular HDAC Activity. All aminoanilide HDACi's **1a−k** and **2a−f** were assessed for their cytotoxicity and HDAC inhibitory activity in

DOI: 10.1021/acs.jmedchem.9b01489
J. Med. Chem. 2019, 62, 11260−11279

Table 3. HDAC Inhibition of Compounds 1a−k and 2a−f[a]

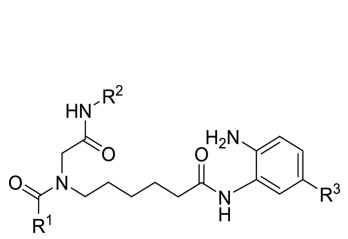

1a-h

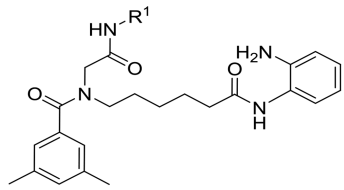

1i-k

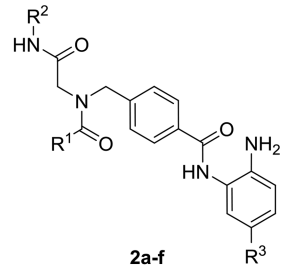

2a-f

compd	R^1	R^2	R^3	HDACi IC_{50} [μM] A2780	Cal27
1a	Ph	c-Hex	H	43.6	21.9
1b	3,5-Me-Ph	c-Hex	H	22.8	12.1
1c	4-Me_2N-Ph	Bn	H	9.25	4.33
1d	3,5-Me-Ph	Bn	H	8.71	3.93
1e	1-naphthyl	c-Hex	H	33.1	13.0
1f	1-naphthyl	Bn	H	10.2	4.13
1g	4-Me_2N-Ph	Bn	F	13.4	6.82
1h	3,5-Me-Ph	Bn	Ph	1.43	0.47
1i	3,5-Me-Ph	4-MeO-Bn	H	3.53	4.81
1j	3,5-Me-Ph	4-Me-Bn	H	4.48	4.57
1k	3,5-Me-Ph	3,5-Me-Bn	H	3.17	3.15
2a	4-Me_2N-Ph	Bn	H	0.48	0.11
2b	3,5-Me-Ph	Bn	H	0.81	0.18
2c	3-Pyridyl	Bn	H	1.06	1.01
2d	3,5-Me-Ph	Bn	Ph	1.72	0.63
2e	4-Me_2N-Ph	Bn	Ph	2.62	0.85
2f	3,5-Me-Ph	Bn	F	1.43	0.47
vorinostat				0.96	0.86

[a]Values are the mean of three experiments. Standard deviations are <10% of the mean. n.e. = no effect up to 100 μM.

Table 4. Inhibitory Activities (IC_{50} [μM]) of Compounds 1h, 2a, 2d and Vorinostat against HDAC1−HDAC4, HDAC6, and HDAC8

compd	IC_{50} [μM] HDAC1	HDAC2	HDAC3	HDAC4	HDAC6	HDAC8
1h	0.057 ± 0.005	1.81 ± 0.12	20% at 10 μM[a]	>10	>10	>10
2a	0.038 ± 0.012	0.283 ± 0.028	0.586 ± 0.055	>10	>10	9.21 ± 0.62
2d	0.051 ± 0.011	34% at 3.33 μM[a]	14% at 10 μM[a]	>10	>10	3.13 ± 0.21
vorinostat	0.111 ± 0.015	0.146 ± 0.014	0.0097 ± 0.0008	42.2 ± 1.2	0.102 ± 0.009	11.9 ± 0.89

[a]% inhibition at the concentration stated (μM).

the human ovarian cancer cell line A2780 and the human tongue squamous cell carcinoma cell line Cal27. Results are summarized in Tables 2 and 3.

The compounds revealed cytotoxic activity with IC_{50} values in the range of 1.60 up to 181 μM (and two compounds, **2d** and **2e**, with no effect up to 100 μM) depending on their substitution pattern and the cell line investigated. In the whole cell HDAC assay, the compounds showed HDAC inhibitory activity from a lower nanomolar range (0.11 μM) up to 43.6 μM. Overall, data from both assays (pIC_{50} values MTT and cellular HDAC assays) show significant correlation (A2780: r^2, 0.7236; Cal27: r^2, 0.6816). **2a** and **2b** were the most potent compounds in both MTT and cellular HDAC assays. **2a** and **2b** were nearly equally cytotoxic in the corresponding cell lines (IC_{50} of 1.60 μM in Cal27 and IC_{50} of 2.40 and 2.80 μM in A2780). In Cal27, **2a** and **2b** were even more potent than the reference pan-HDACi vorinostat in the MTT (1.7-fold) and cellular HDAC assay (~5-fold). Whereas **2a** and **2b** inhibit HDAC1 and HDAC2 with similar potency (Table 1), only **2a**, but not **2b**, potently inhibits HDAC3. Thus, for potent cytotoxicity (MTT assay), inhibition of HDAC1 and HDAC2 seems to be sufficient in the cellular model used in this study. However, HDAC1 inhibition only (no HDAC2 inhibition) reduces cytotoxic potency significantly, as can be seen by comparison of **2b** (HDAC1 and HDAC2 inhibitor) with **2d** or **2e** (both selective HDAC1 inhibitors): in MTT assays at Cal27 cells, **2b** has an IC_{50} of 1.6 μM whereas **2d** and **2e** show IC_{50} values of 8.90 and 11.1 μM, respectively. These findings are in agreement with literature reports on redundant functions of HDAC1 and HDAC2 in gene ablation experiments: combined ablation of HDAC1 and HDAC2 resulted in severe proliferation defects.[13] However, in other cancer cells, knockdown of HDAC3 led to growth inhibition and apoptosis.[20] Thus, even though our results suggest a major role for HDAC1 and HDAC2 (and not HDAC3) in Cal27 and

DOI: 10.1021/acs.jmedchem.9b01489
J. Med. Chem. 2019, 62, 11260−11279

A2780 cells, an important contribution of HDAC3 inhibition cannot be ruled out for other cancer types.

Selection of Hit Compounds and Extended HDAC Isoform Profile of 1h, 2a, and 2d. Based on the high inhibitory activity against HDAC1 in the enzyme assay (Table 1) and on different selectivity profiles, we chose compounds **1h** (HDAC1 selective inhibitor with mediocre HDAC2 and MTT activity), **2a** (most potent compound against HDAC1 and HDAC2 as well as the highest activity in the cellular HDAC and MTT assay), and **2d** (HDAC1 selective inhibitor with low HDAC2 and HDAC3 activity and mediocre activity in the MTT assay) for further analysis. Aminoanilides are typically inactive against class IIa isoforms. To confirm this, **1h**, **2a**, and **2d** were screened for activity against the representative class IIa isoform HDAC4. Furthermore, all three compounds were tested for their inhibition of the remaining class I isoform HDAC8. As expected, **1h**, **2a**, and **2d** displayed only very weak inhibitory activity against HDAC4 and HDAC8 (Table 4). The inhibition data of **1h**, **2a**, and **2d** against HDAC1−HDAC4, HDAC6, and HDAC8 are summarized in Table 4. Taken together, the HDAC isoform profiling discloses compounds **1h** and **2d** as HDAC1 preferential inhibitors and compound **2a** as a potent HDAC1 inhibitor with weaker but submicromolar inhibitory activity against HDAC2 and HDAC3.

Enhancement of Cisplatin-Induced Cytotoxicity. The expression of HDACs is dysregulated in many types of cancers and contributes to the development of drug resistance.[14] Therefore, the combination of chemotherapeutics such as cisplatin with HDACi's could serve as a strategy to overcome chemoresistance. First, we analyzed the effect of the HDACi **1h**, **2a**, or **2d**, respectively, on the cytotoxic potency of cisplatin in cancer cell lines. Cal27 and Cal27CisR were chosen as model systems for cisplatin-sensitive and cisplatin-resistant cell lines.[15] Both cell lines were incubated with 5 μM **1h**, 0.5 μM **2a**, or 3.2 μM **2d** 48 h prior to cisplatin administration for another 72 h followed by MTT readout. Concentrations of **1h**, **2a**, and **2d** were chosen according to cytotoxic effects determined in validation experiments (MTT assays, data not shown). IC_{50} values for cisplatin alone and in combination with **1h**, **2a**, or **2h** together with the corresponding shift factors are shown in Table 5.

Preincubation for 48 h with **1h**, **2a**, or **2d** prior to cisplatin showed a significant enhancement of cisplatin-induced cytotoxicity. In the parental cell line Cal27, a hypersensitization for cisplatin was achieved with all three compounds. Shift factors of sensitization ranged from 5.26 for **1h** up to 7.77 for **2a** and were even higher than those obtained with the pan HDACi vorinostat (shift factor 5.00). Observed shift factors in the cisplatin-resistant subline Cal27CisR were slightly lower than in Cal27 with the exception of vorinostat. **2a** (the most potent compound in MTT, cellular HDAC, and enzyme HDAC assays) gave the highest shift factors (7.77 in Cal27; 7.51 in Cal27CisR) and was able to completely reverse cisplatin resistance in Cal27CisR by shifting the cisplatin IC_{50} from 63.2 μM (without **2a**) to 8.42 μM (presence of 0.5 μM **2a**), which is slightly below the cisplatin IC_{50} value of the native cell line Cal27. In addition, **2a** is even superior to vorinostat in resensitization of Cal27CisR toward cisplatin (shift factor **2a**: 7.51; shift factor vorinostat: 6.73). Figure 5 shows the effect of the most potent compound **2a** on the cytotoxic activity of cisplatin in Cal27CisR cells.

Table 5. IC_{50} Values (μM) after Treatment of Cal27 and Cal27CisR with Cisplatin or in Combination with 5 μM 1h, 0.5 μM 2a, 3.2 μM 2d, or 0.5 μM Vorinostat[a,b]

	Cell line			
	Cal27		Cal27CisR	
compound	IC_{50}	SF	IC_{50}	SF
cisplatin	9.79*		63.2*	
cisplatin + **1h** (5.0 μM)	1.86	5.26	15.7	4.03
cisplatin + **2a** (0.5 μM)	1.26	7.77	8.42	7.51
cisplatin + **2d** (3.2 μM)	1.86	5.26	12.0	5.27
cisplatin + vorinostat (0.5 μM)	1.96	5.00	9.39	6.73

[a]SF means shift factor and was calculated as the ratio of the IC_{50} of cisplatin alone and the IC_{50} of the corresponding drug combination. [b]Data shown are the mean of pooled data from at least three experiments each carried out in triplicate. The standard deviations are <10% of the mean. All shift factors are significant (t test, $p < 0.05$). *IC_{50} value is higher than reported in Table 3 due to different incubation times here: 48 h preincubation with **1h**, **2a**, or **2d** followed by addition of cisplatin and incubation for 72 h.

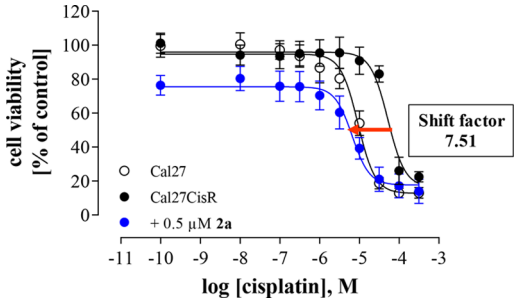

Figure 5. **2a** induces complete resensitization of Cal27CisR cells against cisplatin. Cal27CisR cells were pretreated with 0.5 μM **2a** 48 h prior to application of cisplatin. After another 72 h, IC_{50} values were determined by the MTT assay. The shift factor is defined as the ratio of the IC_{50} of cisplatin alone and the IC_{50} of the corresponding combination with **2a**. Data shown are the mean ± SEM of three independent experiments each performed in triplicate.

To determine the type of interaction between cisplatin and **1h**, **2a**, or **2d**, concentration−effect analyses were performed. The concentrations used for a 48 h preincubation prior to cisplatin for **1h**, **2a**, and **2d** were the same for Cal27 and Cal27CisR, while the cisplatin concentrations were selected based on the IC_{50} values for each cell line. Table 6 shows the CI (combination index) values based on the synergy quantification using the Chou−Talalay method.[16]

The combination index analysis revealed synergistic interaction of **1h**, **2a**, and **2d** with cisplatin (CIs < 0.9). For **1h**, the fraction affected at lower concentrations was frequently less than 0.20 and thus not eligible for analysis. Strong synergism as defined by CI values below 0.20 occurred mostly for **2a**, which is in accordance with the observed higher shift factors for **2a** in comparison to **1h** and **2d**.

Enhancement of Cisplatin-Induced Apoptosis. Next, we examined if the increased cisplatin cytotoxicity induced by **1h**, **2a**, or **2d** is mediated by increased apoptosis. Cal27 and Cal27CisR cells were treated for 48 h with 5 μM **1h**, 0.5 μM **2a**, or 3.2 μM **2d**. Then, cisplatin was added for another 24 h in a concentration corresponding to IC_{50} values from a 72 h MTT assay (Cal27: 3 μM; Cal27CisR: 25 μM), and the subG1 fraction of nuclei was estimated by flow cytometry. Results are shown in Figure 6.

DOI: 10.1021/acs.jmedchem.9b01489
J. Med. Chem. 2019, 62, 11260−11279

Table 6. Interactions between 1h, 2a, or 2d and Cisplatin[a]

	Cal27				Cal27 CisR		
	1h [μM]				**1h** [μM]		
cisplatin [μM]	1.00	3.20	5.00	cisplatin [μM]	1.00	3.20	5.00
0.10	*	*	*	1.00	*	*	*
0.32	*	*	*	3.20	*	*	*
1	*	*	0.76	10	*	*	**0.10**
3.2	*	0.25	**0.10**	32	*	**0.74**	**0.10**
10	0.53	**0.12**	**0.09**	100	**0.06**	**0.09**	**0.05**
	2a [μM]				**2a** [μM]		
cisplatin [μM]	0.10	0.25	0.50	cisplatin [μM]	0.10	0.25	0.50
0.10	*	0.56	0.40	1.00	*	0.76	0.33
0.32	*	0.39	0.32	3.20	*	0.44	0.25
1	0.91	**0.11**	**0.16**	10	*	0.23	**0.12**
3.2	0.37	**0.07**	**0.07**	32	*	**0.04**	**0.03**
10	0.33	**0.02**	**0.07**	100	**0.07**	**0.03**	**0.07**
	2d [μM]				**2d** [μM]		
cisplatin [μM]	0.50	1.00	3.20	cisplatin [μM]	0.50	1.00	3.20
0.10	0.50	0.42	0.39	1.00	0.77	*	*
0.32	0.70	0.52	0.34	3.20	*	0.81	0.89
1	0.59	0.46	0.23	10	0.76	0.50	0.31
3.2	0.21	**0.20**	**0.14**	32	*	0.27	**0.18**
10	**0.18**	**0.16**	**0.08**	100	**0.10**	**0.08**	**0.19**

[a]Cal27 and the cisplatin-resistant tumor cell line Cal27CisR were treated with increasing concentrations of cisplatin and **1h**, **2a**, or **2d**. Data shown are CI (combination index) values calculated using CalcuSyn 2.1 software based on the Chou−Talalay method. A CI > 1 indicates antagonism, a CI = 1 indicates an additive effect, and a CI < 1 indicates synergism. CI < 0.2 indicates strong synergism and is marked in bold. * = fraction affected (fa) less than 0.20.

2a and **2d** activated apoptosis in Cal27 and Cal27CisR as single treatment, whereas **1h** showed no effect on the subG1 population in both cell lines. The apoptosis induction of **2a** and **2d** was similar to that of cisplatin (Cal27: cisplatin, 8.32 ± 0.71%, **2a**, 9.42 ± 1.56%, **2d**, 6.27 ± 0.70%; Cal27CisR: cisplatin, 8.62 ± 0.82%, **2a**, 6.15 ± 1.01%, **2d**, 7.45 ± 0.49%). The combination of **1h**, **2a**, or **2d** with cisplatin induced a significant increase in apoptosis in comparison to cisplatin alone in both cell lines. **2a** again turned out to be the most potent compound. In Cal27 and Cal27CisR, **2a** plus cisplatin induced a 3.8-fold and 4.3-fold increase in apoptotic nuclei in comparison to a single treatment with cisplatin, respectively. In Cal27, apoptosis induction induced by **2a** plus 3 μM cisplatin was similar to 100 μM cisplatin alone (cisplatin, 100 μM, 31.0 ± 1.11%; **2a** + cisplatin, 3 μM, 31.5 ± 1.14%), whereas in Cal27CisR, **2a** plus 25 μM cisplatin gave a higher value than 100 μM cisplatin alone (cisplatin, 100 μM, 32.1 ± 1.98%; **2a** + cisplatin, 25 μM, 37.7 ± 0.79%).

In addition, the combination treatment markedly elevated caspase-3/7 activity in Cal27 and Cal27CisR. Caspase-3/7 activity was monitored by fluorescence image analysis. Results are shown in Figure 7.

The combination of cisplatin with **1h**, **2a**, or **2d** led to a significant increase in caspase-3/7 activation in Cal27 and Cal27CisR. The incubation with **2a** and **2d** as a single treatment showed an activation of caspase-3/7 in the range of cisplatin alone (Cal27: cisplatin, 7.30 ± 1.16%, **2a**, 12.0 ± 1.06%, **2d**, 9.47 ± 1.02%; Cal27CisR: cisplatin, 7.05 ± 0.90, **2a**, 8.16 ± 0.82, **2d**, 5.96 ± 1.17%), which is in accordance with results of subG1 analysis (apoptosis induction, Figure 6).

The increase in caspase 3/7 activation (Figure 7) and apoptosis induction (subG1, Figure 6) upon combination of cisplatin with **1h**, **2a**, or **2d** indicates synergism between cisplatin and **1h**, **2a**, or **2d.** Adding the effects of the single treatments of cisplatin and of **1h**, **2a**, or **2d** does not reach the caspase 3/7 activation (Figure 7) or subG1-apoptosis induction (Figure 6) of the combined cisplatin−HDACi (**1h**, **2a**, or **2d**) treatment, thus supporting in addition to the combination index analysis a synergistic effect of HDACi **1h**, **2a**, or **2d** and cisplatin.

2a in combination with cisplatin showed the highest activation of caspase-3/7 compared to cisplatin alone (6.6-fold increase in Cal27; 10.3-fold increase in Cal27CisR), again confirming the highest potency of **2a** among the novel HDACi. Caspase-3/7 activity of all combination treatments was

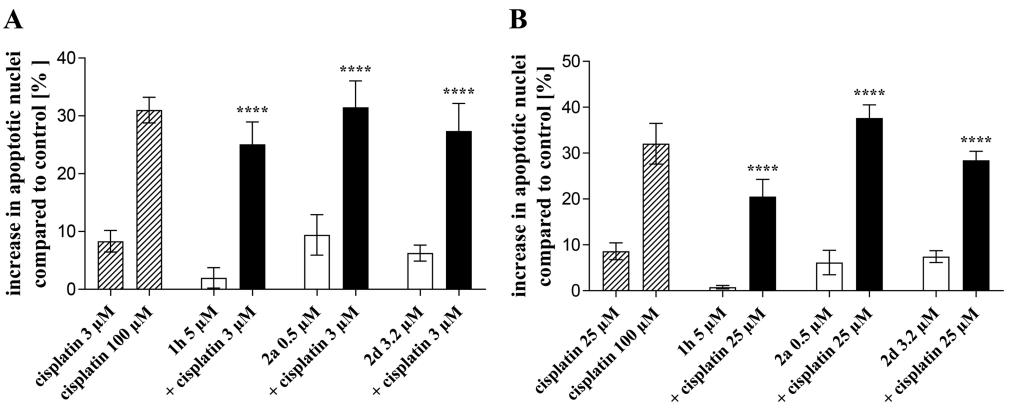

Figure 6. 1h, **2a**, and **2d** enhance cisplatin-induced apoptosis in (A) Cal27 and (B) Cal27CisR cells. Cells were preincubated with 5 μM **1h**, 0.5 μM **2a**, or 3.2 μM **2d** for 48 h, respectively. Cisplatin was added in an IC_{50} concentration for each cell line (Cal27 3 μM (A), Cal27CisR 25 μM (B)). Cisplatin (100 μM) was used as a control for apoptosis induction. After a further incubation period of 24 h, apoptosis was analysed by determining the sub-G1 cell fractions by flow cytometry. The amount of apoptotic nuclei in the vehicle-treated control (0.05% DMSO) was subtracted from the compound treated samples. White bars depict the incubation of cells with **1h**, **2a**, or **2d** only, whereas black bars show the effects of the combination of **1h**, **2a**, or **2d** with cisplatin. Data are means ± SD, $n = 3$. Statistical analysis to compare the apoptosis induction by cisplatin alone and the combination of cisplatin with **1 h**, **2a**, or **2d** was performed using one-way ANOVA (****$p < 0.0001$).

DOI: 10.1021/acs.jmedchem.9b01489
J. Med. Chem. 2019, 62, 11260−11279

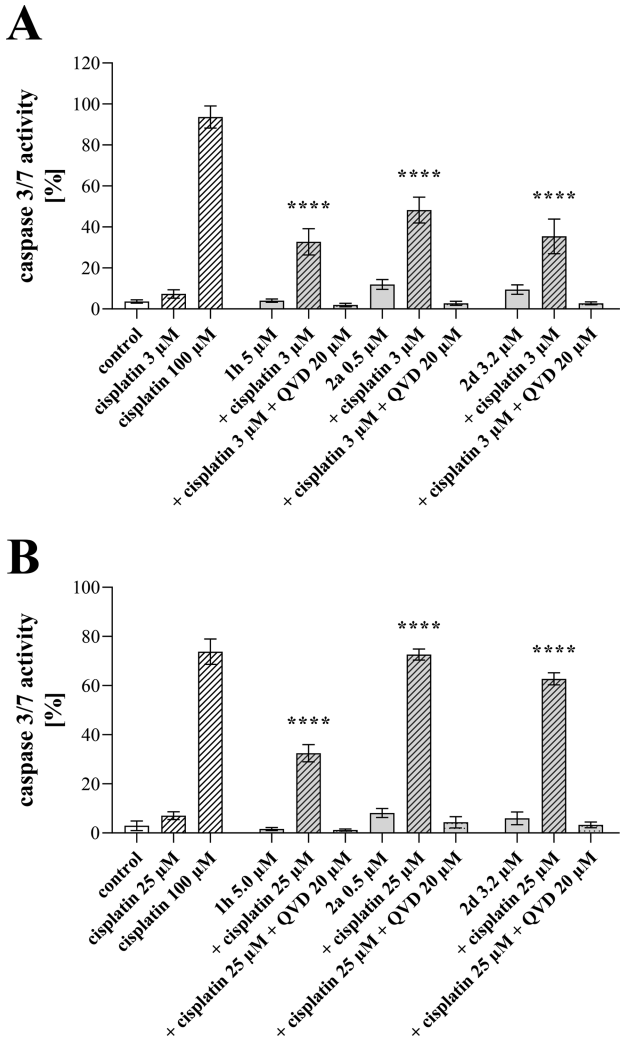

Figure 7. **1h**, **2a**, and **2d** increase cisplatin-induced caspase-3/7 activation. (A) Cal27 and (B) Cal27CisR were treated with the indicated concentrations of **1h**, **2a**, and **2d** for 48 h prior to cisplatin addition (3 μM for Cal27 and 25 μM for Cal27CisR) or buffer control and incubation for another 24 h. The pan caspase inhibitor QVD was used as control. The percentage of (A) Cal27 cells and (B) Cal27CisR cells with activated caspase-3/7 was calculated from the images (shown in Figure S1, Supporting Information). Data are means ± SD. One-way ANOVA was used to compare caspase 3/7 activation by cisplatin alone or the combination of cisplatin and **1h**, **2a**, or **2d** (****$p < 0.0001$).

completely blocked by QVD suggesting specific activation of caspases by the compound treatment.

Accumulation of Acetylated Tubulin and Histone H3. Preincubation with **1h**, **2a**, or **2d** showed a remarkable enhancement of cisplatin potency in caspase activation, apoptosis, and cytotoxicity. To further confirm that the effects of **1h**, **2a**, or **2d** are mediated by HDAC inhibition, the acetylation of histone H3 and α-tubulin was analyzed. Entinostat, nexturastat A, and vorinostat served as controls. Results are shown in Figure 8.

1h, **2a**, and **2d** did not influence the acetylation of α-tubulin after a 24 h incubation. Neither did the HDAC1−HDAC3-selective HDACi entinostat (E). These results confirmed that **1h**, **2a**, and **2d** showed no HDAC6 inhibition in both cell lines. In contrast, the pan-HDACi vorinostat (V) and HDAC6-selective inhibitor nexturastat A (N) showed significant acetylation of α-tubulin in Cal27 and Cal27CisR. However, **1h**, **2a**, and **2d** induced a hyperacetylation of histone H3 similar to entinostat (E) and vorinostat (V) in Cal27 and similar to entinostat (E) in Cal27 CisR. These observed effects underline class I HDAC inhibition for all three compounds. Surprisingly, vorinostat induced only a slight increase in histone H3 acetylation in Cal27CisR whereas the class I-selective HDACi's clearly increase ac-histone H3.

CONCLUSIONS

This work describes efficient and versatile synthetic protocols for the preparation of peptoid-based HDACi's with 2-aminoanilide groups as the ZBG. To this end, we applied a convenient Ugi 4-component reaction or straightforward submonomer pathways followed by the introduction of the ZBG to synthesize a library of peptoid-based HDACi's. All synthesized compounds were screened for their inhibitory activity on HDAC1−HDAC3 and HDAC6, inhibition of cellular HDAC activity, and cytotoxicity in the human ovarian cancer cell line A2780 and the human squamous carcinoma cell line Cal27. As expected, all compounds demonstrated inhibitory activity on recombinant HDAC1, HDAC2, and/or HDAC3 (class I) and were inactive against the class IIb isoform HDAC6. Docking studies were able to correctly predict the ligands' capabilities to inhibit the HDAC isoforms 1, 2, and 3. Western blot experiments confirmed the selective inhibition of class I HDACs in a cellular environment.

On the basis of anticancer activity and the HDAC selectivity profile, compounds **1h**, **2a**, and **2d** were selected to investigate their activity against cisplatin-resistant cancer cells (Cal27-CisR). Cisplatin resistance is a complex phenomenon and the major factor for therapy failure besides toxic side effects of cisplatin. Mechanisms of cisplatin resistance include alterations in the cellular accumulation (decreased influx or increased efflux of cisplatin), intracellular detoxification (glutathione or metallothionein conjugation), and activated DNA damage repair or damage tolerance.[17,18] Combination therapies could be a promising approach to resensitize cancer toward cisplatin. It has already been shown by our group and others that a combination of an HDACi and cisplatin has a synergistic antitumor effect in hematological and solid tumors.[11,19,21,22] By leading to an open chromatin structure, HDACi's increase the transcription of key genes involved in the regulation of cell proliferation, cell cycle, and apoptosis,[19−21] eventually resulting in the reestablishment of cisplatin sensitivity.

All three compounds were able to enhance the cisplatin-induced cytotoxicity and to resensitize the Cal27CisR cells toward cisplatin. The results from this study highlight once more the utility of class I-selective HDACi's in comparison to pan HDACi to resensitize cisplatin resistant cancer cells as we have recently shown with entinostat for high-grade serous ovarian cancer cell lines (HGSOC).[21] HDAC1 selective inhibitors (**1h**, **2d**), or HDAC1−HDAC3 inhibitors (**2a**), are all able to reverse cisplatin resistance, increase caspase 3/7 activation, and increase apoptosis in a synergistic manner. The most potent HDACi, **2a** with nanomolar activity at HDAC1−HDAC3 and the highest cytotoxicity (higher than vorinostat), showed the largest shift factors for reversing cisplatin resistance in a cellular model of platinum resistance. We previously identified dual class I/class IIb inhibitors that are able to enhance the cisplatin sensitivity in Cal27CisR cells.[11,22] Importantly, this study provides for the first time evidence for the treatment of HNSCC that pan-HDAC inhibition or

DOI: 10.1021/acs.jmedchem.9b01489
J. Med. Chem. 2019, 62, 11260−11279

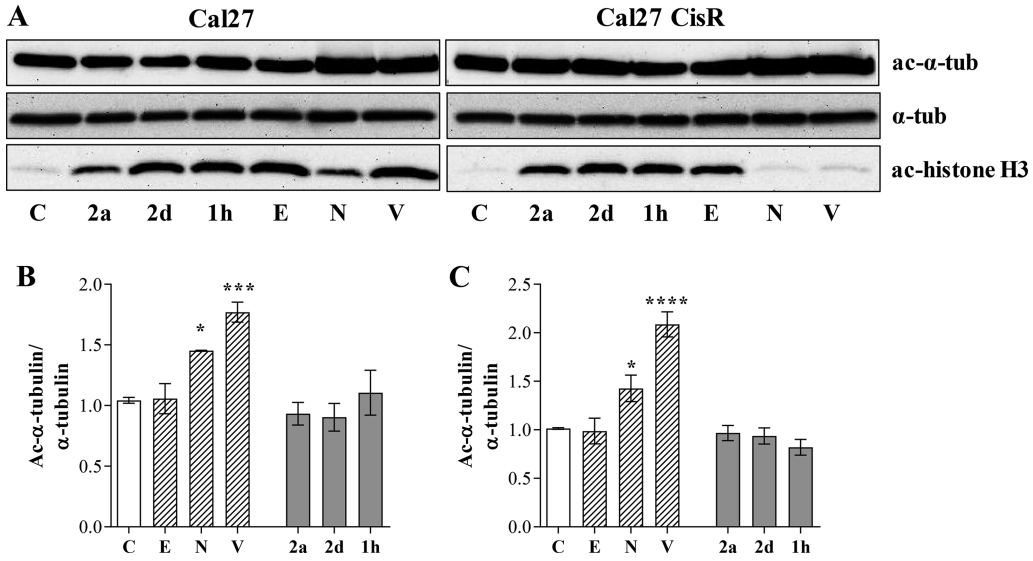

Figure 8. Compound-induced α-tubulin and histone H3 acetylation in Cal27 and Cal27CisR. (A) Representative immunoblot analysis of acetylated α-tubulin (ac-α-tub), α-tubulin (α-tub), and acetylated histone H3 (ac-histone H3). Cal27 and Cal27CisR were incubated for 24 h with the vehicle as control (C, 0.05% DMSO), 0.5 μM **2a**, 3.2 μM **2d**, 5 μM **1 h**, 1 μM entinostat (E), 1 μM nexturastat A (N), or 1 μM vorinostat (V), respectively. Densitometric analysis of tubulin acetylation in (B) Cal27 or (C) Cal27CisR was performed by ImageJ software (NIH). All values have been normalized to α-tubulin. Statistical analysis was performed using one-way ANOVA (*$p < 0.05$, ***$p < 0.001$, ****$p < 0.0001$).

dual class I/class IIb inhibition is not required for full reversal of cisplatin resistance. Taken together, the concept of regaining chemosensitivity by applying epigenetic modulators, here class I-selective HDACi's, is further corroborated by this study.

EXPERIMENTAL SECTION

Chemistry. *General Section.* Methyl 6-aminohexanoate hydrochloride,[23] 2-bromo-*N*-(4-methoxybenzyl)acetamide,[24] *tert*-butyl-(2-aminophenyl)carbamate,[25] *tert*-butyl-(4-bromo-2-nitrophenyl)-carbamate,[26] *tert*-butyl-(3-nitro-[1,1′-biphenyl]-4-yl)carbamate,[27] *tert*-butyl-(2-amino-4-fluorophenyl)carbamate,[28] and *tert*-butyl-(3-amino-[1,1′-biphenyl]-4-yl)carbamate[29] were prepared according to published procedures. All other chemicals and solvents were obtained from commercial suppliers (Sigma-Aldrich, Acros Organics, Carbolution Chemicals) and used as purchased without further purification. The progress of all reactions was monitored by thin-layer chromatography (TLC) using Merck precoated silica gel plates (with fluorescence indicator UV_{254}). Components were visualized by irradiation with ultraviolet light (254 nm) or staining in potassium permanganate solution. Flash column chromatography was performed using a prepacked silica cartridge with the solvent mixtures specified in the corresponding experiment. Melting points (mp) were taken in open capillaries on a Mettler FP 5 melting-point apparatus and are uncorrected. Proton (^{1}H) and carbon (^{13}C) NMR spectra were recorded on a Bruker Avance 300, 500, or 600 using DMSO-d_6, MeOH-d_4, or $CDCl_3$ as solvents. Chemical shifts are given in parts per million (ppm), relative to the residual solvent peak for ^{1}H and ^{13}C. ^{1}H NMR signals marked with an asterisk (*) correspond to peaks assigned to the minor rotamer conformation. Elemental analysis was performed on a Perkin Elmer PE 2400 CHN elemental analyzer. High-resolution mass spectra (HRMS) analysis was performed on a UHR-TOF maXis 4G, Bruker Daltonics, Bremen by electrospray ionization (ESI). Analytical HPLC analyses were carried out on a Varian Prostar system equipped with a Prostar 410 (autosampler), 210 (pumps), and 330 (UV-detector) using a Phenomenex Luna 5u C18(2) 1.8 μm particle (250 mm × 4.6 mm) column, supported by Phenomenex Security Guard Cartridge Kit C18 (4.0 mm × 3.0 mm). UV absorption was detected at 254 nm with a linear gradient of 10% A to 100% A in 20 min using HPLC-grade water + 0.1% TFA (solvent B) and HPLC-grade acetonitrile + 0.1% TFA (solvent A) for elution at a flow rate of 1 mL/min. The purity of all final compounds was 95% or higher.

General Procedures. *General Procedure for the Synthesis of the Compounds **1a–k** and **2a–f**.* The Boc-protected compounds **4a–h**, **7**, **11a,b**, and **13a–f** (0.1 mmol, 1 equiv) were dissolved in a 15% solution of TFA in dichloromethane (5 mL) and stirred for 30 min at RT. After completion of the reaction, saturated sodium carbonate solution was added until no bubble formation was visible. The reaction solution was extracted with dichloromethane (3 × 15 mL) and washed with 1 M sodium hydroxide (3 × 10 mL) and brine (3 × 10 mL). Subsequently, the collected organic extracts were dried over sodium sulfate and the solvent was removed under reduced pressure. The product was precipitated out of *n*-hexane and ethyl acetate.

*General Procedure for the Synthesis of the Compounds **3a–h** and **12a–f**.* A mixture of methyl 6-aminohexanoate hydrochloride (153 mg, 0.8 mmol, 1.2 equiv), *para*-formaldehyde (25 mg, 0.8 mmol, 1.2 equiv), triethylamine (116 μL, 0.8 mmol, 1.2 equiv), and 150 mg of crushed molecular sieves (MS, 4 Å) was stirred in dry methanol (2 mL, 0.5 M) for 30 min at RT. Subsequently, the appropriate carboxylic acid (1.0 mmol, 1.0 equiv) and, after further 10 min, the isocyanide (1.0 mmol, 1.0 equiv) were added and stirred for 24 h at RT. After completion of the reaction, the reaction mixture was filtered and the solvent was removed under reduced pressure. The crude products were purified by flash chromatography (prepacked silica cartridge, *n*-hexane–ethyl acetate, gradient: 100:00 → 50:50 in 30 min) and crystallized from ethyl acetate/*n*-hexane to yield the desired products **3a–h** and **12a–f**. The compound characterization data for **3a–e**, **3g,h**, and **12d–f** were previously published.[11]

*General Procedure for the Synthesis of the Compounds **4a–h, 7, and 11a,b**.* Lithium hydroxide monohydrate (92 mg, 2.2 mmol, 2 equiv) was added to the appropriate ester **3a–h**, **6**, or **10a,b** (1.1 mmol, 1 equiv), dissolved in methanol (5 mL), and stirred for 16 h at RT. After completion of the reaction, the solution was acidified with 1 M HCl to a pH ≈ 1. The reaction solution was extracted with ethyl acetate (3 × 20 mL) and washed with brine (3 × 20 mL). The solvent was removed under reduced pressure. The appropriate Boc-protected amine (0.9 mmol, 1 equiv) was dissolved in CH_2Cl_2/DMF (1:1, v/v), and pyridine (149 μL, 1.8 mmol, 2 equiv) was added. Subsequently, the appropriate carboxylic acid (1.1 mmol, 1.2 equiv), DIC (170 μL, 1.1 mmol, 1.2 equiv), and HOAt (150 mg, 1.1 mmol, 1.2 equiv) were added and stirred for 24 h at RT. After completion of the reaction, the

DOI: 10.1021/acs.jmedchem.9b01489
J. Med. Chem. 2019, 62, 11260–11279

reaction solution was extracted with ethyl acetate (3 × 20 mL) and washed with brine (3 × 20 mL). The combined organic extracts were dried over sodium sulfate. The crude products were purified by flash chromatography (prepacked silica cartridge, *n*-hexane−ethyl acetate, gradient: 100:00 → 40:60 in 30 min) and precipitated out of *n*-hexane and ethyl acetate.

General Procedure for the Synthesis of Compounds ***10a,b.*** Compound 7 (984 mg, 2.5 mmol, 1 equiv) was dissolved in 6 mL of a 20% TFA solution in dichloromethane. The solution was stirred for 2 h at RT. After completion of the reaction, the solvent was removed under reduced pressure. The residue was treated with toluene (2 × 3 mL), which was subsequently removed under reduced pressure. The residue was partly (360 mg, 1.1 mmol, 1 equiv) dissolved in DMF/CH_2Cl_2 (1:1, v/v, 5 mL). EDC·HCl (205 mg, 2.2 mmol, 2 equiv) and DMAP (52 mg, 0.4 mmol, 0.4 equiv) were added to the solution. Subsequently, the appropriate amine (1.1 mmol, 1 equiv) was added and stirred for 16 h. After completion of the reaction, the solution was extracted with ethyl acetate (3 × 20 mL) and washed with brine (3 × 20 mL). The solvent was removed under reduced pressure. The crude products were purified by flash chromatography (prepacked silica cartridge, *n*-hexane−ethyl acetate, gradient 100:00 → 50:50 in 30 min), and the products were precipitated out of ethyl acetate and *n*-hexane.

General Procedure for the Synthesis of the Compounds 13a−f. Lithium hydroxide monohydrate (48 mg, 1.1 mmol, 2 equiv) was added to the appropriate ester **12a−f** (0.6 mmol, 1 equiv), dissolved in methanol (5 mL), and stirred for 16 h at RT. After completion of the reaction, the solution was acidified with 1 M HCl to pH ≈ 1 and extracted with ethyl acetate (3 × 20 mL). The solvent was removed under reduced pressure. To the appropriate carboxylic acid (0.6 mmol, 1 equiv) in CH_2Cl_2:DMF (1:1, v/v) were added EDC·HCl (218 mg, 1.1 mmol, 2.4 equiv) and DMAP (28 mg, 0.4 mmol, 0.4 equiv) and stirred for 10 min. Subsequently, the appropriate Boc-protected amine (0.6 mmol, 1 equiv) was added to the reaction and stirred for further 24 h at RT. After completion of the reaction, the solution was extracted with ethyl acetate (3 × 20 mL) and washed with brine (3 × 20 mL). The crude products were purified by flash chromatography (prepacked silica cartridge, *n*-hexane−ethyl acetate, gradient: 100:00 → 40:60 in 30 min) and precipitated out of *n*-hexane and ethyl acetate.

Compound Characterization Data. *N-{6-[(2-Aminophenyl)amino]-6-oxohexyl}-N-[2-(cyclohexylamino)-2-oxoethyl]-benzamide (**1a**).* White solid; 52%; mp 144 °C; t_R = 11.81 min, 98.5% purity; ^{1}H NMR (600 MHz, DMSO-d_6) δ 9.11/9.04* (s, 1H), 7.81−6.52 (m, 10H), 4.81/4.78* (s, 2H), 4.01*/3.74 (s, 2H), 3.56−3.16 (m, 3H), 2.33/2.22* (t, J = 7.0 Hz, 2H), 1.75−1.07 (m, 16H). ^{13}C NMR (151 MHz, DMSO-d_6) δ 171.2, 171.1, 167.1, 141.9, 136.9, 129.2, 129.2, 128.4, 128.3, 126.5, 126.4, 125.8, 125.4, 123.6, 116.3, 116.0, 51.5, 49.6, 47.7, 47.3, 45.9, 35.8, 35.6, 32.5, 32.3, 27.6, 26.4, 26.2, 25.7, 25.3, 24.9, 24.6, 24.5. HRMS (ESI) [M + H]$^+$: 465.2868, calcd for $C_{27}H_{37}N_4O_3$: 465.2860.

*N-{6-[(2-Aminophenyl)amino]-6-oxohexyl}-N-[2-(cyclohexylamino)-2-oxoethyl]-3,5-dimethylbenzamide (**1b**).* White solid; 63%; mp 85 °C; t_R = 12.58 min, 98.6% purity; ^{1}H NMR (600 MHz, DMSO-d_6) δ 9.09/9.02* (s, 1H), 7.78*/7.74 (d, J = 7.7 Hz, 1H), 7.16−6.51 (m, 7H), 4.81/4.78* (s, 2H), 3.98*/3.73 (s, 2H), 3.58−3.49 (m, 1H), 3.37−3.16 (m, 2H), 2.34−2.24 (m, 8H), 1.75−1.09 (m, 16H). ^{13}C NMR (151 MHz, DMSO-d_6) δ 171.13, 171.05, 167.2, 141.89, 141.86, 137.52, 137.51, 137.3, 136.8, 133.1, 130.4, 125.7, 125.7, 125.3, 125.2, 124.0, 123.96, 123.6, 116.2, 115.9, 51.4, 51.3, 47.6, 47.6, 45.9, 45.8, 35.7, 35.6, 32.5, 32.3, 27.5, 27.3, 26.4, 26.2, 25.64, 25.62, 25.20, 25.15, 24.9, 24.8, 24.6, 24.5, 20.8. HRMS (ESI) [M + H]$^+$: 493.3178, calcd for $C_{29}H_{40}N_4O_3$: 493.3173.

*N-{6-[(2-Aminophenyl)amino]-6-oxohexyl}-N-[2-(benzylamino)-2-oxoethyl]-4-(dimethylamino)benzamide (**1c**).* White solid; 42%; mp 139 °C; t_R = 9.30 min, 95.1% purity; ^{1}H NMR (600 MHz, DMSO-d_6) δ 9.22 (bs, 1H), 8.54 (bs, 1H), 7.33−6.51 (m, 13H), 4.85 (s, 2H), 4.31 (d, J = 5.7 Hz, 2H), 4.00 (m, 2H), 2.92 (s, 6H), 2.36−2.25 (m, 2H), 1.60−1.15 (m, 6H). ^{13}C NMR (151 MHz, DMSO-d_6) δ 171.3, 171.1, 168.6, 150.9, 141.8, 139.4, 128.4, 128.3, 127.2, 126.8, 125.6, 125.2, 123.6, 116.1, 115.8, 110.9, 42.1, 40.1, 39.7, 35.6, 26.0, 25.5, 25.1. HRMS (ESI) [M + H]$^+$: 516.2971, calcd for $C_{30}H_{38}N_5O_3$: 516.2969.

*N-{6-[(2-Aminophenyl)amino]-6-oxohexyl}-N-[2-(benzylamino)-2-oxoethyl]-3,5-dimethyl-benzamide (**1d**).* White solid; 60%; mp 147 °C; t_R = 12.83 min, 96.4% purity; ^{1}H NMR (600 MHz, DMSO-d_6) δ 9.11/9.05* (s, 1H), 8.44−8.43 (m, 1H), 7.32−6.52 (m, 12H), 4.82/4.79* (s, 2H), 4.34*/4.27 (d, J = 5.6 Hz, 2H), 4.08*/3.86 (s, 2H), 3.40−3.20 (m, 2H), 2.35−2.22 (m, 8H), 1.64−1.12 (m, 6H). ^{13}C NMR (151 MHz, DMSO-d_6) δ 171.1, 171.1, 168.2, 141.88, 141.85, 139.4, 139.2, 137.5, 137.4, 136.7, 136.5, 130.50, 130.45, 128.28, 128.25, 127.23, 127.15, 126.9, 126.7, 125.7, 125.3, 125.2, 124.04, 123.98, 123.6, 123.5, 116.2, 115.9, 51.4, 49.7, 47.5, 45.8, 42.2, 42.1, 35.7, 35.6, 27.6, 26.3, 26.1, 25.6, 25.2, 24.8, 20.8. HRMS (ESI) [M + H]$^+$: 501.2866, calcd for $C_{30}H_{37}N_4O_3$: 501.2860.

*N-{6-[(2-Aminophenyl)amino]-6-oxohexyl}-N-[2-(cyclohexylamino)-2-oxoethyl]-1-naphthamide (**1e**).* White solid; 80%; mp 171 °C; t_R = 13.10 min, 98.4% purity; ^{1}H NMR (600 MHz, DMSO-d_6) δ 9.12*/8.98 (s, 1H), 8.21−6.51 (m, 12H), 4.83*/4.76 (s, 2H), 4.48−2.97 (m, 5H), 2.38*/2.13 (t, J = 7.4 Hz, 2H), 1.82−0.94 (m, 16H). ^{13}C NMR (151 MHz, DMSO-d_6) δ 171.1, 170.9, 170.02, 169.99, 166.9, 166.7, 141.9, 141.8, 134.8, 134.6, 133.0, 132.8, 129.2, 129.0, 128.6, 128.2, 128.1, 126.8, 126.5, 126.3, 125.7, 125.4, 125.28, 125.25, 125.2, 125.1, 124.7, 123.6, 123.5, 123.4, 116.2, 116.1, 115.88, 115.86, 50.9, 49.1, 47.7, 47.5, 46.7, 45.7, 35.7, 35.5, 32.5, 32.2, 27.5, 26.6, 26.3, 25.5, 25.23, 25.18, 25.1, 24.8, 24.6, 24.4. HRMS (ESI) [M + H]$^+$: 515.3021, calcd for $C_{31}H_{39}N_4O_3$: 515.3017.

*N-{6-[(2-Aminophenyl)amino]-6-oxohexyl}-N-[2-(benzylamino)-2-oxoethyl]-1-naphthamide (**1f**).* White solid; 81%; mp 148 °C; t_R = 12.73 min, 97.7% purity; ^{1}H NMR (600 MHz, DMSO-d_6) δ 9.13*/8.98 (m, 1H), 8.58/8.23* (t, J = 5.9 Hz, 1H), 8.17−6.51 (m, 16H), 4.83*/4.76 (s, 2H), 4.52−3.01 (m, 6H), 2.39*/2.14 (t, J = 7.4 Hz, 2H), 1.75−0.97 (m, 6H). ^{13}C NMR (151 MHz, DMSO-d_6) δ 171.1, 170.9, 170.1, 170.0, 168.2, 167.9, 141.9, 141.8, 139.3, 139.0, 134.7, 134.5, 132.8, 131.5, 129.2, 128.6, 128.6, 128.3, 128.2, 127.3, 127.2, 126.84, 126.81, 126.5, 126.4, 125.7, 125.7, 125.33, 125.29, 125.24, 125.21, 123.59, 123.58, 123.5, 116.1, 115.9, 52.1, 50.9, 49.3, 47.0, 42.2, 42.0, 35.7, 35.5, 27.6, 26.6, 26.3, 25.5, 25.2, 24.8. HRMS (ESI) [M + H]$^+$: 523.2702, calcd for $C_{32}H_{35}N_4O_3$: 523.2704.

*N-{6-[(2-Amino-5-fluorophenyl)amino]-6-oxohexyl}-N-[2-(benzylamino)-2-oxoethyl]-4-(dimethylamino)benzamide (**1g**).* Greyish solid; 70%; mp 76 °C; t_R = 10.38 min, 95.9% purity; ^{1}H NMR (600 MHz, DMSO-d_6) δ 9.08 (s, 1H), 8.45 (s, 1H), 7.33−6.64 (m, 12H), 4.77 (s, 2H), 4.31 (d, J = 5.7 Hz, 2H), 4.06−3.92 (m, 2H), 2.92 (s, 6H), 2.36−2.28 (m, 2H), 1.58−1.15 (m, 6H). ^{13}C NMR (151 MHz, DMSO-d_6) δ 171.3, 171.2, 168.6, 154.5, 153.0, 150.9, 139.4, 137.2, 128.4, 128.3, 127.2, 126.8, 124.4, 124.3, 123.0, 116.1, 116.0, 111.4, 111.2, 110.9, 110.6, 110.5, 110.4, 42.1, 40.1, 39.7, 35.8, 26.0, 25.0, 23.3. HRMS (ESI) [M + H]$^+$: 534.2882, calcd for $C_{30}H_{37}FN_5O_3$: 534.2875.

*N-{6-[(4-Amino-[1,1′-biphenyl]-3-yl)amino]-6-oxohexyl}-N-[2-(benzylamino)-2-oxoethyl]-3,5-dimethylbenzamide (**1h**).* Brown solid; 79%; mp 92 °C; t_R = 14.68 min, 98.6% purity; ^{1}H NMR (600 MHz, DMSO-d_6) δ 9.18/9.11* (s, 1H), 8.47−8.39 (m, 1H), 7.56−6.80 (m, 16H), 5.03/5.00* (s, 2H), 4.34*/4.28 (d, J = 5.3 Hz, 2H), 4.09*/3.87 (s, 2H), 3.42−3.21 (m, 2H), 2.39−2.21 (m, 8H), 1.67−1.14 (m, 6H). ^{13}C NMR (151 MHz, DMSO-d_6) δ 171.28, 171.25, 171.14, 171.10, 168.21, 168.19, 141.4, 140.3, 139.4, 139.2, 137.4, 137.4, 136.7, 136.5, 130.5, 130.4, 128.8, 128.27, 128.25, 128.1, 127.2, 127.1, 126.9, 126.7, 126.0, 125.5, 124.04, 123.98, 123.9, 123.8, 123.28, 123.25, 116.2, 51.4, 49.7, 47.5, 45.8, 42.17, 42.07, 35.8, 35.7, 27.7, 26.3, 26.2, 25.6, 25.1, 24.8, 20.8. HRMS (ESI) [M + H]$^+$: 577.3175, calcd for $C_{36}H_{40}N_4O_3$: 577.3173.

*N-{6-[(2-Aminophenyl)amino]-6-oxohexyl}-N-{2-[(4-methoxybenzyl)amino]-2-oxoethyl}-3,5-dimethylbenzamide (**1i**).* Grayish solid; 57%; mp 168 °C; t_R = 12.17 min, 96.7% purity; ^{1}H NMR (500 MHz, DMSO-d_6) δ 9.08/9.02* (s, 1H), 8.36−8.29 (m, 1H), 7.22−6.51 (m, 11H), 4.80/4.77* (s, 2H), 4.26*/4.20 (d, J = 4.7 Hz, 2H), 4.06*/3.83, 3.72 (s, 3H), 3.42−3.17 (m, 2H), 2.34−2.21 (m, 8H), 1.63−1.09 (m, 6H). ^{13}C NMR (126 MHz, DMSO-d_6) δ

DOI: 10.1021/acs.jmedchem.9b01489
J. Med. Chem. 2019, 62, 11260−11279

171.0, 170.9, 168.0, 158.2, 141.8, 137.3, 130.4, 128.6, 128.4, 125.6, 125.1, 123.9, 123.6, 116.1, 115.8, 113.6, 55.0, 51.4, 49.6, 47.4, 45.7, 41.6, 41.5, 35.7, 35.6, 27.6, 26.3, 26.1, 25.6, 25.1, 24.8, 20.7. HRMS (ESI) $[M + H]^+$: 531.2968, calcd for $C_{31}H_{38}N_4O_4$: 531.2966.

N-{6-[(2-Aminophenyl)amino]-6-oxohexyl}-3,5-dimethyl-N-{2-[(4-methylbenzyl)amino]-2-oxoethyl}benzamide (**1j**). Brown solid; 91%; mp 81 °C; t_R = 13.07 min, 96.1% purity; ^{1}H NMR (600 MHz, DMSO-d_6) δ 9.10/9.03* (s, 1H), 8.38−8.37 (m, 1H), 7.17−6.52 (m, 11H), 4.82−4.79 (m, 2H), 4.28*/4.22 (d, J = 5.2 Hz, 2H), 4.07*/3.84, 3.40−3.19 (m, 2H), 2.35−2.22 (m, 11H) 1.64−1.12 (m, 6H). ^{13}C NMR (151 MHz, DMSO-d_6) δ 171.1, 170.9, 168.1, 141.87, 141.85, 137.5, 137.4, 136.7, 136.4, 136.2, 135.9, 135.8, 130.49, 130.45, 128.8, 127.3, 127.2, 125.7, 125.3, 125.2, 124.03, 123.98, 123.58, 123.55, 116.2, 115.9, 51.4, 49.7, 47.5, 45.8, 41.92, 41.85, 35.7, 35.6, 27.6, 26.3, 26.1, 25.6, 25.2, 24.8, 20.8, 20.7. HRMS (ESI) $[M + H]^+$: 515.3021, calcd for $C_{31}H_{38}N_4O_3$: 515.3017.

N-{6-[(2-Aminophenyl)amino]-6-oxohexyl}-N-{2-[(3,5-dimethylbenzyl)amino]-2-oxo-ethyl}-3,5-dimethylbenzamide (**1k**). White solid; 82%; mp 83 °C; t_R = 13.82 min, 96.0% purity; ^{1}H NMR (600 MHz, DMSO-d_6) δ 9.10/9.03* (s, 1H), 8.36−8.35 (m, 1H), 7.17−6.52 (m, 10H), 4.81/4.78* (s, 2H), 4.25*/4.19 (d, J = 4.2 Hz, 2H), 4.07*/3.84 (s, 2H), 3.39−3.21 (m, 2H), 2.34−2.21 (m, 14H), 1.63−1.12 (m, 6H). ^{13}C NMR (151 MHz, DMSO-d_6) δ 171.1, 170.9, 168.1, 141.9, 139.2, 138.9, 137.5, 137.4, 137.23, 137.17, 136.7, 136.5, 130.5, 130.4, 128.3, 128.1, 125.7, 125.3, 125.2, 125.0, 124.0, 123.6, 123.5, 116.2, 115.9, 51.4, 49.7, 47.5, 45.7, 42.2, 42.0, 35.7, 35.6, 27.6, 26.3, 26.2, 25.6, 25.2, 24.8, 20.9, 20.8, 20.7. HRMS (ESI) $[M + H]^+$: 529.3178, calcd for $C_{32}H_{40}N_4O_3$: 529.3173.

N-{4-[(2-Aminophenyl)carbamoyl]benzyl}-N-[2-(benzylamino)-2-oxoethyl]-4-(dimethyl-amino)benzamide (**2a**). White solid; 82%; mp 128 °C; t_R = 9.98 min, 95.8% purity; ^{1}H NMR (500 MHz, DMSO-d_6) δ 9.64 (s, 1H), 8.47−8.41 (m, 1H), 8.00−6.60 (m, 17H), 4.88 (s, 2H), 4.73 (s, 2H), 4.33 (d, J = 5.7 Hz, 2H), 3.93 (s, 2H), 2.94 (s, 6H). ^{13}C NMR (126 MHz, DMSO-d_6) δ 171.7, 168.1, 165.0, 151.2, 143.0, 141.0, 139.2, 133.5, 128.5, 128.2, 128.0, 127.2, 126.8, 126.6, 126.4, 123.3, 116.2, 116.1, 110.9, 42.1. HRMS (ESI) $[M + H]^+$: 536.2654, calcd for $C_{32}H_{34}N_5O_3$: 536.2656.

N-{4-[(2-Aminophenyl)carbamoyl]benzyl}-N-[2-(benzylamino)-2-oxoethyl]-3,5-dimethyl-benzamide (**2b**). White solid; 74%; mp 110 °C; t_R = 13.08 min, 95.2% purity; ^{1}H NMR (600 MHz, DMSO-d_6) δ 9.67−9.66 (m, 1H), 8.46*/8.42 (t, J = 5.8 Hz, 1H), 7.99−6.59 (m, 16H), 4.90 (s, 2H), 4.73/4.60* (s, 2H), 4.34*/4.29 (d, J = 5.8 Hz, 2H), 4.01*/3.81 (s, 2H), 2.26−2.25 (m, 6H). ^{13}C NMR (151 MHz, DMSO-d_6) δ 171.61, 171.59, 167.8, 167.6, 165.1, 164.9, 143.2, 143.1, 140.8, 140.4, 139.3, 139.1, 137.64, 137.61, 136.0, 135.9, 133.7, 133.6, 130.9, 130.8, 128.32, 128.28, 128.2, 128.1, 127.6, 127.24, 127.16, 126.9, 126.83, 126.78, 126.7, 126.5, 124.14, 124.08, 123.31, 123.26, 116.3, 116.1, 53.2, 51.0, 48.7, 47.4, 42.2, 42.1, 28.0, 20.8. HRMS (ESI) $[M + H]^+$: 536521.2551, calcd for $C_{32}H_{32}N_4O_3$: 521.2547.

N-{4-[(2-Aminophenyl)carbamoyl]benzyl}-N-[2-(benzylamino)-2-oxoethyl]nicotinamide (**2c**). White solid; 75%; mp 120 °C; t_R = 8.87 min, 95.4% purity; ^{1}H NMR (600 MHz, DMSO-d_6) δ 9.68 (s, 1H), 8.69−6.59 (m, 18H), 4.90 (s, 2H), 4.75/4.65* (s, 2H), 4.35*/4.26 (d, J = 5.4 Hz, 2H), 4.09*/3.89 (s, 2H). ^{13}C NMR (151 MHz, DMSO-d_6) δ 169.5, 169.3, 167.6, 167.4, 165.0, 164.9, 150.7, 150.5, 147.4, 147.1, 143.2, 140.4, 140.1, 139.3, 138.8, 134.5, 133.8, 133.6, 132.0, 131.7, 128.33, 128.30, 128.25, 128.0, 127.7, 127.22, 127.17, 126.9, 126.8, 126.7, 126.5, 123.6, 123.4, 123.32, 123.25, 116.3, 116.1, 53.4, 51.2, 49.1, 48.2, 42.3, 42.1. HRMS (ESI) $[M + H]^+$: 494.2192, calcd for $C_{29}H_{28}N_5O_3$: 494.2187.

N-{4-[(4-Amino-[1,1′-biphenyl]-3-yl)carbamoyl]benzyl}-N-[2-(benzylamino)-2-oxoethyl]-3,5-dimethylbenzamide (**2d**). White/rose solid; 65%; mp 124 °C; t_R = 15.75 min, 97.6% purity; ^{1}H NMR (600 MHz, DMSO-d_6) δ 9.76*/9.75 (s, 1H), 8.47*/8.43 (t, J = 5.6 Hz, 1H), 8.03−6.87 (m, 20H), 5.11 (s, 2H), 4.74/4.62* (s, 2H), 4.34*/4.29 (d, J = 5.7 Hz, 2H), 4.02*/3.82 (s, 2H), 2.25 (s, 6H). ^{13}C NMR (151 MHz, DMSO-d_6) δ 171.62, 171.60, 167.8, 167.7, 165.2, 165.1, 142.84, 142.77, 140.9, 140.2, 139.3, 139.1, 137.6, 136.0, 135.9, 133.7, 133.5, 130.9, 130.8, 128.8, 128.32, 128.28, 128.25, 128.1, 128.1, 127.6, 127.3, 127.2, 126.9, 126.84, 126.78, 126.0, 125.5, 124.82, 124.76, 124.7, 124.2, 124.1, 123.6, 123.5, 116.5, 53.2, 51.0, 48.7, 47.5, 42.2, 42.1, 20.8. HRMS (ESI) $[M + H]^+$: 597.2859, calcd for $C_{38}H_{37}N_4O_3$: 597.2860.

N-{4-[(4-Amino-[1,1′-biphenyl]-3-yl)carbamoyl]benzyl}-N-[2-(benzylamino)-2-oxoethyl]-4-(dimethylamino)benzamide (**2e**). Rose solid; 75%; mp 122 °C; t_R = 12.75 min, 95.8% purity; ^{1}H NMR (600 MHz, DMSO-d_6) δ 9.74 (s, 1H), 8.48 (bs, 1H), 8.02−6.65 (m, 21H), 5.10 (s, 2H), 4.73 (bs, 2H), 4.32 (d, J = 5.8 Hz, 2H), 3.93 (bs, 2H), 2.94 (s, 6H). ^{13}C NMR (151 MHz, DMSO-d_6) δ 171.8, 168.2, 165.2, 151.3, 142.8, 141.1, 140.2, 139.3, 133.5, 128.8, 128.6, 128.3, 128.1, 127.3, 126.9, 126.0, 125.5, 124.8, 124.7, 123.6, 116.5, 111.0, 42.1. HRMS (ESI) $[M + H]^+$: 612.2967, calcd for $C_{38}H_{37}N_5O_3$: 612.2969.

N-{4-[(2-Amino-5-fluorophenyl)carbamoyl]benzyl}-N-[2-(benzylamino)-2-oxoethyl]-3,5-dimethylbenzamide (**2f**). White solid; 88%; mp 211 °C; t_R = 13.60 min, 95.1% purity; ^{1}H NMR (600 MHz, DMSO-d_6) δ 9.68*/9.66 (s, 1H), 8.46*/8.42 (t, J = 5.7 Hz, 1H), 7.98−6.77 (m, 15H), 4.85 (s, 2H), 4.74/4.61* (s, 2H), 4.34*/4.29 (d, J = 5.7 Hz, 2H), 4.01*/3.81 (s, 2H), 2.25 (s, 6H). ^{13}C NMR (151 MHz, DMSO-d_6) δ 171.6, 167.8, 167.6, 165.2, 165.0, 154.6, 153.0, 141.0, 140.7, 139.3, 139.1, 139.0, 138.9, 137.64, 137.62, 136.0, 135.8, 133.5, 133.3, 130.9, 130.8, 128.32, 128.28, 128.2, 128.1, 127.7, 127.3, 127.2, 126.91, 126.88, 126.78, 124.14, 124.09, 116.62, 116.57, 112.7, 112.6, 112.44, 112.35, 112.3, 112.2, 53.2, 51.0, 48.7, 47.5, 42.2, 42.1, 20.8. HRMS (ESI) $[M + H]^+$: 539.2450, calcd for $C_{32}H_{32}FN_4O_3$: 539.2453.

Methyl 6-{N-[2-(Benzylamino)-2-oxoethyl]-1-naphthamido}-hexanoate (**3f**). White solid; 90%; mp 91 °C; ^{1}H NMR (600 MHz, DMSO-d_6) δ 8.57/8.22* (t, J = 5.9 Hz, 1H), 8.23−7.05 (m, 12H), 4.48−2.99 (m, 9H), 2.37*/2.06 (t, J = 7.3 Hz, 2H), 1.70−0.91 (m, 6H). ^{13}C NMR (151 MHz, DMSO-d_6) δ 173.4, 173.1, 170.0, 168.2, 167.9, 139.3, 139.0, 134.7, 134.5, 133.0, 132.8, 129.2, 128.9, 128.6, 128.6, 128.3, 128.2, 128.1, 127.24, 127.17, 126.9, 126.8, 126.5, 126.4, 125.3, 124.6, 125.20, 125.17, 123.6, 123.5, 51.2, 51.1, 50.9, 49.2, 47.1, 45.6, 42.2, 42.0, 33.2, 32.8, 27.3, 26.4, 26.0, 25.1, 24.3, 23.7. Anal calcd for $C_{27}H_{30}N_2O_4$: C 72.62, H 6.77, N 6.27. Found: C 72.55, H 6.88, N 6.14.

tert-Butyl-[2-(6-{N-[2-(cyclohexylamino)-2-oxoethyl]-benzamido}hexanamido)phenyl]carbamate (**4a**). White solid; 71%; mp 94 °C; t_R = 17.92 min, 96.6% purity; ^{1}H NMR (600 MHz, DMSO-d_6) δ 9.44/9.37* (s, 1H), 8.34/8.30* (s, 1H), 7.80−7.76 (m, 1H), 7.53−7.05 (m, 8H), 4.01*/3.74 (s, 2H), 3.57−3.51 (m, 1H), 3.38−3.16 (m, 2H), 2.37/2.25* (t, J = 7.0 Hz, 2H), 1.76−1.08 (m, 25H).^{13}C NMR (151 MHz, DMSO-d_6) δ 171.7, 171.5, 170.9, 170.8, 167.0, 166.8, 153.1, 153.0, 136.8, 136.6, 131.1, 131.0, 129.7, 129.6, 129.1, 128.3, 128.2, 126.5, 126.3, 125.0, 124.8, 123.8, 123.6, 79.3, 51.4, 49.6, 47.6, 47.3, 45.8, 45.7, 35.9, 35.7, 32.4, 32.2, 28.1, 27.5, 26.4, 26.2, 26.0, 25.9, 25.5, 25.2, 25.14, 25.05, 24.7, 24.54, 24.45, 24.29. HRMS (ESI) $[M + H]^+$: 565.3386, calcd for $C_{32}H_{45}N_4O_5$: 565.3384.

tert-Butyl-[2-(6-{N-[2-(cyclohexylamino)-2-oxoethyl]-3,5-dimethylbenzamido}hexanamido)phenyl]carbamate (**4b**). White solid; 70%; mp 88 °C; t_R = 19.45 min, 97.5% purity; ^{1}H NMR (500 MHz, DMSO-d_6) δ 9.41/9.34* (s, 1H), 8.30/8.27* (s, 1H), 7.74−7.69 (m, 1H), 7.54−6.92 (m, 7H), 3.99*/3.73 (s, 2H), 3.60−3.50 (m, 1H), 3.37−3.17 (m, 2H), 2.37−2.24 (m, 8H), 1.76−1.10 (m, 25H). ^{13}C NMR (126 MHz, DMSO-d_6) δ 171.6, 171.4, 170.9, 167.0, 166.8, 153.0, 137.3, 137.2, 136.8, 136.6, 131.0, 130.3, 129.6, 124.9, 124.7, 123.9, 123.7, 123.5, 79.2, 51.3, 49.4, 47.5, 47.1, 45.7, 35.8, 32.1, 28.0, 27.4, 26.2, 25.9, 25.4, 25.1, 24.9, 24.6, 24.3, 20.6. HRMS (ESI) $[M + H]^+$: 593.3700, calcd for $C_{34}H_{49}N_4O_5$: 593.3697.

tert-Butyl-[2-(6-{N-[2-(benzylamino)-2-oxoethyl]-4-(dimethylamino)benzamido}hexanamido)phenyl]carbamate (**4c**). White solid; 56%; mp 94 °C; t_R = 13.97 min, 95.2% purity; ^{1}H NMR (600 MHz, DMSO-d_6) δ 9.43 (s, 1H), 8.45 (bs, 1H), 8.33 (s, 1H), 7.55−6.64 (m, 13H), 4.31 (d, J = 5.8 Hz, 2H), 3.98 (bs, 2H), 3.35−3.33 (m, 2H), 2.38−2.29 (m, 2H), 1.59−1.25 (m, 15H). ^{13}C NMR (151 MHz, DMSO-d_6) δ 171.5, 171.2, 168.5, 153.0, 150.9, 139.3, 131.0, 129.6, 128.4, 128.3, 128.1, 127.1, 126.7, 124.9, 124.7, 123.7,

DOI: 10.1021/acs.jmedchem.9b01489
J. Med. Chem. 2019, 62, 11260−11279

123.5, 123.0, 110.8, 79.2, 42.1, 35.8, 33.5, 28.0, 25.8, 24.8, 24.1. HRMS (ESI) $[M + H]^+$: 616.3496, calcd for $C_{36}H_{46}N_5O_5$: 616.3493.

*tert-Butyl-[2-(6-{N-[2-(benzylamino)-2-oxoethyl]-3,5-dimethylbenzamido}hexanamido)phenyl]carbamate (**4d**).* White solid; 61%; mp 73 °C; t_R = 17.40 min, 95.4% purity; ^{1}H NMR (600 MHz, DMSO-d_6) δ 9.44/9.38* (s, 1H), 8.42 (t, J = 5.7 Hz, 1H), 8.34/8.30* (s, 1H), 7.53−6.92 (m, 12H), 4.33*/4.27 (d, J = 5.5 Hz, 2H), 4.07*/3.85 (s, 2H), 3.40−3.18 (m, 2H), 2.38−2.21 (m, 2H), 1.68−1.12 (m, 15H). ^{13}C NMR (151 MHz, DMSO-d_6) δ 171.7, 171.5, 171.13, 171.08, 168.2, 153.1, 153.0, 139.4, 139.2, 137.4, 137.4, 136.7, 136.5, 131.1, 131.0, 130.49, 130.46, 129.7, 129.6, 128.28, 128.25, 127.24, 127.16, 126.9, 126.7, 125.0, 124.8, 124.01, 123.98, 123.8, 123.6, 79.3, 79.3, 51.4, 49.7, 47.5, 45.8, 42.2, 42.1, 35.9, 35.8, 28.1, 27.6, 26.3, 26.0, 25.5, 25.0, 24.8, 24.7, 20.8. HRMS (ESI) $[M + H]^+$: 601.3385, calcd for $C_{36}H_{45}N_4O_5$: 601.3384.

*tert-Butyl-[2-(6-{N-[2-(cyclohexylamino)-2-oxoethyl]-1-naphthamido}hexanamido)phenyl]carbamate (**4e**).* White solid; 57%; mp 89 °C; t_R = 19.94 min, 96.2% purity; ^{1}H NMR (600 MHz, DMSO-d_6) δ 9.47*/9.30 (s, 1H), 8.36*/8.26 (s, 1H), 8.19−7.04 (m, 12H), 4.47−2.97 (m, 5H), 2.42*/2.16 (t, J = 7.2 Hz, 2H), 1.81−0.94 (m, 25H). ^{13}C NMR (151 MHz, DMSO-d_6) δ 171.7, 171.5, 170.00, 169.98, 166.8, 166.7, 153.1, 153.0, 134.8, 134.5, 133.0, 132.8, 131.1, 131.0, 129.7, 129.6, 129.2, 129.0, 128.6, 128.6, 128.3, 128.1, 126.8, 126.5, 126.3, 125.4, 125.2, 125.1, 125.01, 124.99, 124.9, 124.8, 124.7, 123.9, 123.8, 123.6, 123.4, 79.4, 79.3, 50.9, 49.1, 47.7, 47.5, 46.7, 45.7, 36.0, 35.7, 32.5, 32.2, 28.1, 28.0, 27.5, 26.6, 26.2, 25.4, 25.2, 25.10, 25.06, 24.61, 24.56, 24.4. HRMS (ESI) $[M + H]^+$: 615.3550, calcd for $C_{36}H_{47}N_4O_5$: 615.3541.

*tert-Butyl-[2-(6-{N-[2-(benzylamino)-2-oxoethyl]-1-naphthamido}hexanamido)phenyl]carbamate (**4f**).* White solid; 71%; mp 93 °C; t_R = 18.66 min, 96.2% purity; ^{1}H NMR (600 MHz, DMSO-d_6) δ 9.47*/9.31 (s, 1H), 8.58/8.23* (t, J = 5.9 Hz), 8.36*/8.27 (s, 1H), 8.16−7.04 (m, 17H), 4.51−3.02 (m, 6H), 2.42*/2.15 (t, J = 7.2 Hz, 2H), 1.75−0.98 (m, 15H). ^{13}C NMR (151 MHz, DMSO-d_6) δ 171.8, 171.5, 170.1, 170.0, 168.2, 167.9, 153.1, 153.0, 139.3, 139.0, 134.7, 134.5, 133.0, 132.8, 131.1, 131.0, 129.7, 129.6, 129.2, 128.9, 128.7, 128.6, 128.3, 128.2, 128.2, 127.3, 127.2, 126.9, 126.8, 126.5, 126.4, 125.3, 125.19, 125.17, 125.0, 124.9, 124.8, 124.6, 123.9, 123.8, 123.6, 123.5, 79.4, 79.3, 50.9, 49.4, 47.1, 45.8, 42.2, 42.1, 36.0, 35.7, 28.1, 28.0, 27.6, 26.6, 26.2, 25.4, 25.1, 24.6. HRMS (ESI) $[M + H]^+$: 565.3386, calcd for $C_{32}H_{45}N_4O_5$: 565.3384.

*tert-Butyl-[2-(6-{N-[2-(benzylamino)-2-oxoethyl]-4-dimethylamino}benzamido)hexanamido]-4-fluorophenylcarbamate (**4g**).* White solid; 70%; mp 85 °C; t_R = 14.65 min, 95.0% purity; ^{1}H NMR (600 MHz, DMSO-d_6) δ 9.36 (s, 1H), 8.51−8.38 (m, 2H), 7.50−6.63 (m, 12H), 4.31 (d, J = 5.6 Hz, 2H), 3.98 (bs, 2H), 2.92 (s, 6H), 2.38−2.30 (m, 2H), 1.58−1.17 (m, 15H). ^{13}C NMR (151 MHz, DMSO-d_6) δ 171.6, 171.3, 168.5, 159.2, 157.3, 153.3, 150.9, 139.3, 131.9, 128.3, 128.17, 127.18, 126.7, 126.2, 125.7, 123.0, 110.9, 110.7, 79.3, 42.1, 36.0, 28.0, 27.2, 25.8, 24.7. HRMS (ESI) $[M + H]^+$: 634.3410, calcd for $C_{35}H_{45}FN_5O_5$: 634.3399.

*tert-Butyl-[3-(6-{N-[2-(benzylamino)-2-oxoethyl]-3,5-dimethylbenzamido}hexanamido)-[1,1′-biphenyl]-4-yl]carbamate (**4h**).* Rose solid; 68%; mp 138 °C; ^{1}H NMR (600 MHz, DMSO-d_6) δ 9.52/9.45* (s, 1H), 8.47−8.43 (m, 2H), 7.77−6.92 (m, 16H), 4.34*/4.27 (d, J = 5.2 Hz, 2H), 4.09*/3.86 (s, 2H), 3.41−3.22 (m, 2H), 2.42−2.20 (m, 2H), 1.67−1.15 (m, 15H). ^{13}C NMR (151 MHz, DMSO-d_6) δ 171.9, 171.7, 171.1, 171.10, 168.20, 168.17, 153.1, 153.0, 139.4, 139.2, 137.4, 136.7, 136.5, 135.6, 130.5, 130.4, 129.9, 129.0, 128.27, 128.25, 127.3, 127.24, 127.16, 126.9, 126.7, 126.3, 124.02, 123.98, 123.84, 123.84, 123.2, 122.8, 79.5, 51.4, 49.7, 47.6, 45.8, 42.2, 42.1, 36.0, 35.9, 28.1, 27.7, 26.3, 26.0, 25.5, 25.0, 24.7, 20.8. HRMS (ESI) $[M + H]^+$: 677.3702, calcd for $C_{41}H_{49}N_4O_5$: 677.3697. Anal calcd for $C_{41}H_{48}N_4O_5$: C 72.76, H 7.15, N 8.28. Found: C 72.52, H 7.36, N 7.99.

*Methyl 6-(N-{2-[(4-Methoxybenzyl)amino]-2-oxoethyl}-3,5-dimethylbenzamido)hexanoate (**6**).* Methyl 6-aminohexanoate hydrochloride (1.8 g, 9.9 mmol, 1 equiv) was dissolved in dichloromethane (30 mL) at 0 °C, and triethylamine (2.75 mL, 19.8 mmol, 2 equiv) was added. Subsequently, 2-bromo-*N*-(4-methoxybenzyl)acetamide (2.56 g, 9.9 mmol, 1 equiv) was added and stirred for 16 h at RT. After completion of the reaction, the solution was extracted with dichloromethane (3 × 30 mL) and washed with water (3 × 30 mL) and brine (3 × 30 mL). The secondary amine **5** (2.26 g, 7.0 mmol, 1.2 equiv) was directly used in a reaction with pyridine (566 μL, 7.0 mmol, 1.2 equiv) in dichloromethane at 0 °C. Subsequently, 3,5-dimethylbenzoyl-chloride (864 μL, 5.8 mmol, 1 equiv) was added and stirred for 16 h at RT. The reaction solution was extracted with dichloromethane (3 × 20 mL) and washed with water (3 × 20 mL) and 1 M hydrochloric acid (3 × 10 mL). The product **6** was precipitated out of ethyl acetate and *n*-hexane. White solid; 57%; mp 59 °C; ^{1}H NMR (600 MHz, DMSO-d_6) δ 8.35−8.34 (m, 1H), 7.21−6.85 (m, 7H), 4.25*/4.19 (d, J = 5.4 Hz, 2H), 4.04*/3.81 (s, 2H), 3.72 (s, 3H), 3.59/3.56* (s, 3H), 3.36−3.15 (m, 2H), 2.33−2.18 (m, 8H), 1.56−1.04 (m, 6H). ^{13}C NMR (151 MHz, DMSO-d_6) δ 173.3, 173.2, 171.1, 168.0, 158.3, 158.2, 137.4, 137.4, 136.7, 136.5, 131.4, 131.2, 130.5, 128.6, 128.5, 124.0, 113.7, 55.1, 51.4, 51.2, 49.5, 47.5, 45.6, 41.6, 41.5, 33.2, 33.0, 27.3, 26.1, 25.8, 25.3, 24.2, 23.8, 20.8. Anal calcd for $C_{26}H_{34}N_2O_5$: C 68.70, H 7.54, N 6.16. Found: C 68.67, H 7.75, N 6.23.

*tert-Butyl-{2-[6-(N-{2-[(4-methoxybenzyl)amino]-2-oxoethyl}-3,5-dimethylbenzamido)hexanamido]phenyl}carbamate (**7**).* White solid; 60%; mp 77 °C; t_R = 18.48 min, 99.5% purity; ^{1}H NMR (600 MHz, DMSO-d_6) δ 9.44/9.38* (s, 1H), 8.35−8.30 (m, 2H), 7.53−6.85 (m, 11H), 4.26*/4.19 (d, J = 4.8 Hz, 2H), 4.05*/3.82 (s, 2H), 3.71 (s, 3H), 3.39−3.20 (m, 2H), 2.38−2.21 (m, 8H), 1.64−1.12 (m, 15H). ^{13}C NMR (151 MHz, DMSO-d_6) δ 171.7, 171.6, 171.11, 171.07, 168.02, 167.99, 158.3, 158.2, 153.1, 137.44, 137.40, 136.7, 136.5, 131.3, 131.2, 131.1, 130.5, 129.7, 128.7, 128.5, 125.0, 124.8, 124.0, 123.8, 123.6, 113.7, 79.33, 79.31, 55.0, 51.4, 49.7, 47.5, 45.8, 41.63, 41.55, 35.9, 35.8, 28.1, 27.6, 26.3, 26.0, 25.5, 25.0, 24.7, 20.8. HRMS (ESI) $[M + H]^+$: 631.3489, calcd for $C_{36}H_{46}N_4O_6$: 631.3490.

*Methyl 6-{N-[2-(tert-Butoxy)-2-oxoethyl]-3,5-dimethylbenzamido}hexanoate (**9**).* To a solution of methyl 6-aminohexanoate hydrochloride (2.9 g, 16.1 mmol, 1 equiv) in tetrahydrofuran (30 mL), triethylamine (4.5 mL, 32.2 mmol, 2 equiv) was added and stirred for 10 min at RT. Subsequently, *tert*-butyl-bromoacetate (2.4 mL, 16.1 mmol, 1 equiv) was added and stirred for further 16 h at RT. After completion of the reaction, the solvent was removed under reduced pressure. The crude product **8** (3.76 g, 14.5 mmol, 1.2 equiv) was dissolved in dichloromethane (20 mL) at 0 °C. Pyridine (1.2 mL, 14.5 mmol, 1.2 equiv) and 3,5-dimethylbenzoylchloride (1.8 mL, 12.1 mmol, 1 equiv) were added, and the solution was stirred for 18 h at RT. The solvent was removed under reduced pressure. The crude product was purified by flash chromatography (prepacked silica cartridge, *n*-hexane−ethyl acetate, gradient: 100:00 → 50:50 in 30 min). Yellowish oil; 57%; t_R = 19.68 min, 97.6% purity; ^{1}H NMR (600 MHz, $CDCl_3$) δ 6.96−6.92 (m, 3H), 4.04/3.78* (s, 2H), 3.61*/3.59 (s, 3H), 3.45*/3.22 (t, J = 7.5 Hz, 2H), 2.30−2.16 (m, 8H), 1.66−1.10 (m, 15H). ^{13}C NMR (151 MHz, $CDCl_3$) δ 174.0, 173.7, 172.4, 172.4, 168.7, 168.3, 138.0, 136.3, 136.0, 131.02, 130.98, 124.2, 124.0, 82.1, 81.7, 51.9, 51.4, 49.9, 47.3, 46.5, 33.9, 33.7, 28.1, 28.1, 28.0, 26.8, 26.5, 25.9, 24.7, 24.3, 21.2. HRMS (ESI) $[M + H]^+$: 392.2434, calcd for $C_{22}H_{34}NO_5$: 392.2431.

*Methyl 6-(3,5-Dimethyl-N-{2-[(4-methylbenzyl)amino]-2-oxoethyl}benzamido)hexanoate (**10a**).* White solid; 71%; mp 78 °C; ^{1}H NMR (600 MHz, DMSO-d_6) δ 8.37−8.36 (m, 1H), 7.18−6.91 (m, 7H), 4.27*/4.22 (d, J = 5.4 Hz, 2H), 4.05*/3.82 (s, 2H), 3.59/3.56* (s, 3H), 3.36−3.16 (m, 2H), 2.33−2.18 (m, 11H), 1.56−1.05 (m, 6H). ^{13}C NMR (126 MHz, DMSO-d_6) δ 173.3, 173.2, 171.1, 168.10, 168.07, 137.44, 137.41, 136.7, 136.5, 136.4, 136.2, 135.9, 135.8, 130.5, 128.8, 127.3, 127.2, 124.0, 51.4, 51.17, 51.15, 49.5, 47.5, 45.6, 41.9, 41.8, 33.2, 33.0, 27.3, 26.1, 25.8, 25.3, 24.2, 23.8, 20.8, 20.7. Anal calcd for $C_{26}H_{34}N_2O_4$: C 71.21, H 7.81, N 6.39; found: C 71.28, H 8.00, N 6.19.

*Methyl 6-(N-{2-[(3,5-Dimethylbenzyl)amino]-2-oxoethyl}-3,5-dimethylbenzamido)hexanoate (**10b**).* White solid; 52%; mp 83 °C; ^{1}H NMR (600 MHz, DMSO-d_6) δ 8.35−8.34 (m, 1H), 7.06−6.81 (m, 6H), 4.25*/4.19 (d, J = 5.4 Hz, 2H), 4.06*/3.83 (s, 2H), 3.59/3.55* (s, 3H), 3.36−3.16 (m, 2H), 2.33−2.18 (m, 14H), 1.56−

DOI: 10.1021/acs.jmedchem.9b01489
J. Med. Chem. 2019, 62, 11260−11279

1.05 (m, 6H). ^{13}C NMR (126 MHz, DMSO-d_6) δ 173.3, 173.2, 171.1, 168.1, 139.2, 138.9, 137.5, 137.4, 137.23, 137.16, 136.7, 136.5, 130.5, 128.3, 128.1, 125.2, 125.0, 124.0, 51.4, 51.2, 51.1, 49.5, 47.5, 45.6, 42.2, 42.0, 33.2, 33.0, 27.3, 26.1, 26.0, 25.3, 24.2, 23.8, 20.9, 20.7. Anal calcd for $C_{27}H_{36}N_2O_4$: C 71.65, H 8.02, N 6.19; found: C 71.49, H 8.11, N 6.11.

*tert-Butyl-{2-[6-(3,5-dimethyl-N-{2-[(4-methylbenzyl)amino]-2-oxoethyl}benzamido)hexanamido]phenyl}carbamate (**11a**).* White solid; 60%; mp 78 °C; ^{1}H NMR (600 MHz, DMSO-d_6) δ 9.45/9.38* (s, 1H), 8.37−8.30 (m, 2H), 7.54−6.92 (m, 11H), 4.28*/4.22 (d, J = 5.3 Hz, 2H), 4.06*/3.83 (s, 2H), 3.40−3.19 (m, 2H), 2.38−2.21 (m, 11H), 1.64−1.12 (m, 15H). ^{13}C NMR (151 MHz, DMSO-d_6) δ 171.7, 171.5, 171.11, 171.08, 168.09, 168.05, 153.1, 153.0, 137.44, 137.40, 136.7, 136.5, 136.4, 136.2, 135.9, 135.8, 131.1, 131.0, 130.47, 130.46, 129.7, 129.6, 128.8, 127.3, 127.2, 125.0, 124.8, 124.0, 123.8, 123.6, 79.33, 79.30, 51.4, 49.7, 47.5, 45.8, 41.92, 41.85, 35.9, 35.8, 28.1, 27.6, 26.3, 26.0, 25.5, 25.0, 24.7, 20.8, 20.6. HRMS (ESI) [M + H]$^+$: 615.3547, calcd for $C_{36}H_{47}N_4O_5$: 615.3541. Anal calcd for $C_{36}H_{46}N_4O_5$: C 70.33, H 7.54, N 9.11; found: C 70.08, H 7.63, N 8.83.

*tert-Butyl-{2-[6-(N-{2-[(3,5-dimethylbenzyl)amino]-2-oxoethyl}-3,5-dimethylbenzamido)hexanamido]phenyl}carbamate (**11b**).* White solid; 59%; mp 75 °C; t_R = 18.92 min, 98.2% purity; ^{1}H NMR (600 MHz, DMSO-d_6) δ 9.44/9.38* (s, 1H), 8.36−8.30 (m, 2H), 7.53−6.81 (m, 10H), 4.25*/4.19 (d, J = 4.9 Hz, 1H), 4.07*/3.84 (s, 2H), 3.39−3.21 (m, 2H), 2.37−2.21 (m, 14H), 1.64−1.13 (m, 15H). ^{13}C NMR (151 MHz, DMSO-d_6) δ 171.7, 171.5, 171.10, 171.07, 168.1, 153.1, 153.0, 139.2, 138.9, 137.44, 137.37, 137.22, 137.16, 136.7, 136.5, 131.1, 130.48, 130.46, 129.6, 128.3, 128.1, 125.2, 125.0, 124.8, 124.0, 123.8, 123.6, 79.33, 79.31, 51.4, 49.7, 47.5, 45.7, 42.2, 42.0, 35.9, 35.8, 28.0, 27.6, 26.3, 26.0, 25.5, 25.0, 24.7, 21.0, 20.8, 20.7. HRMS (ESI) [M + H]$^+$: 629.3697, calcd for $C_{37}H_{49}N_4O_5$: 629.3697.

*Methyl 4-({N-[2-(Benzylamino)-2-oxoethyl]-4-(dimethylamino)-benzamido}methyl)benzoate (**12a**).* White solid; 68%; mp 131 °C; ^{1}H NMR (600 MHz, DMSO-d_6) δ 8.49−8.41 (m, 1H), 7.96−6.64 (m, 13H), 4.71 (bs, 2H), 4.30 (d, J = 5.8 Hz), 3.92 (bs, 2H), 3.85 (s, 3H), 2.93 (s, 6H). ^{13}C NMR (151 MHz, DMSO-d_6) δ 171.8, 168.1, 166.1, 151.2, 143.3, 139.2, 129.4, 128.6, 128.5, 128.3, 128.0, 127.3, 126.8, 122.0, 110.9, 52.1, 51.5, 49.3, 42.1, 39.7. Anal calcd for $C_{27}H_{29}N_3O_4$: C 70.57, H 6.36, N 9.14; found: C 70.44, H 6.45, N 9.04.

*Methyl 4-({N-[2-(Benzylamino)-2-oxoethyl]-3,5-dimethylbenzamido}methyl)benzoate (**12b**).* White solid; 73%; mp 82 °C; ^{1}H NMR (600 MHz, DMSO-d_6) δ 8.45*/8.40 (t, J = 5.7 Hz, 1H), 7.97−7.01 (m, 1H), 4.73/4.60* (s, 2H), 4.33*/4.28 (d, J = 5.8 Hz, 2H), 4.02*/3.82 (s, 2H), 3.86 (s, 3H), 2.26/2.24* (s, 6H). ^{13}C NMR (151 MHz, DMSO-d_6) δ 171.6, 167.8, 167.6, 166.1, 166.0, 143.0, 142.8, 139.3, 139.1, 137.6, 135.9, 135.8, 130.1, 129.5, 129.4, 128.7, 128.5, 128.30, 128.26, 127.9, 127.24, 127.16, 126.9, 126.8, 124.1, 53.3, 52.1, 51.2, 48.8, 47.7, 42.2, 42.1, 20.8. Anal calcd for $C_{27}H_{28}N_2O_4$: C 72.95, H 6.35, N 6.30; found: C 72.97, H 6.35, N 6.21.

*Methyl 4-({N-[2-(Benzylamino)-2-oxoethyl]nicotinamido}-methyl)benzoate (**12c**).* White solid; 78%; mp 105 °C; ^{1}H NMR (600 MHz, DMSO-d_6) δ 8.69−7.12 (m, 14H), 4.74/4.64* (s, 2H), 4.34*/4.24 (d, J = 5.7 Hz, 2H), 4.09*/3.89 (s, 2H), 3.86 (s, 3H). ^{13}C NMR (151 MHz, DMSO-d_6) δ 169.6, 169.4, 167.6, 167.4, 166.1, 166.0, 150.6, 150.5, 147.4, 147.0, 142.6, 142.4, 139.2, 138.8, 134.5, 134.4, 131.9, 131.6, 129.6, 129.4, 128.8, 128.6, 128.3, 128.0, 127.2, 126.9, 126.8, 123.6, 123.4, 53.4, 52.1, 51.4, 49.2, 48.3, 42.3, 42.1. Anal calcd for $C_{24}H_{23}N_3O_4$: C 69.05, H 5.55, N 10.07; found: C 68.84, H 5.72, N 9.76.

*tert-Butyl-{2-[4-({N-[2-(benzylamino)-2-oxoethyl]-4-(dimethylamino)benzamido}methyl)benzamido]phenyl}-carbamate (**13a**).* White solid; 61%; mp 126 °C; ^{1}H NMR (500 MHz, DMSO-d_6) δ 9.82 (s, 1H), 8.64 (s, 1H), 8.43 (t, J = 5.3 Hz, 1H), 7.96−6.65 (m, 17H), 4.73 (s, 2H), 4.32 (d, J = 5.8 Hz, 2H), 3.93 (s, 2H), 2.94 (s, 6H), 1.45(s, 9H). ^{13}C NMR (126 MHz, DMSO-d_6) δ 171.7, 168.1, 165.0, 153.4, 151.2, 141.6, 139.2, 133.1, 131.7, 129.7, 128.5, 128.2, 127.8, 127.2, 126.8, 125.9, 125.5, 124.0, 123.8, 110.9, 79.6, 42.1, 28.0. HRMS (ESI) [M + H]$^+$: 636.3182, calcd for $C_{37}H_{42}N_5O_5$: 636.3180. Anal calcd for $C_{37}H_{41}N_5O_5$: C 69.90, H 6.50, N 11.02; found: C 69.63, H 6.63, N 10.90.

*tert-Butyl-{2-[4-({N-[2-(benzylamino)-2-oxoethyl]-3,5-dimethylbenzamido}methyl)benzamido]phenyl}carbamate (**13b**).* White solid; 62%; mp 122 °C; ^{1}H NMR (500 MHz, DMSO-d_6) δ 9.84 (s, 1H), 8.68 (s, 1H), 8.46*/8.41 (t, J = 5.8 Hz, 1H), 7.97−7.03 (m, 16H), 4.74/4.61* (s, 2H), 4.34*/4.29 (d, J = 5.8 Hz, 2H), 4.02*/3.82 (s, 2H), 2.25 (s, 6H), 1.45 (s, 9H). ^{13}C NMR (126 MHz, DMSO-d_6) δ 171.63, 171.60, 167.8, 167.6, 165.1, 165.0, 153.5, 141.4, 141.1, 139.3, 139.1, 137.6, 136.0, 135.9, 133.3, 133.2, 131.8, 131.7, 130.9, 130.8, 129.7, 128.31, 128.27, 128.0, 127.9, 127.8, 127.3, 127.2, 127.0, 126.9, 126.8, 126.1, 126.0, 125.6, 124.11, 124.08, 123.9, 79.7, 53.2, 51.1, 48.7, 47.5, 42.2, 42.1, 28.0, 20.8. HRMS (ESI) [M + H]$^+$: 621.3067, calcd for $C_{37}H_{41}N_4O_5$: 621.3071. Anal calcd for $C_{37}H_{40}N_4O_5$: C 71.59, H 6.50, N 9.03; found: C 71.16, H 6.71, N 8.76.

*tert-Butyl-{2-[4-({N-[2-(benzylamino)-2-oxoethyl]nicotinamido}-methyl)benzamido]phenyl}carbamate (**13c**).* White solid; 25%; mp 115 °C; t_R = 13.48 min, 96.1% purity; ^{1}H NMR (600 MHz, DMSO-d_6) δ 9.85 (s, 1H), 8.69−8.13 (m, 19H), 4.76/4.66* (s, 2H), 4.35*/4.25 (d, J = 5.4 Hz, 2H), 4.09*/3.89 (s, 2H), 1.44 (s, 9H). ^{13}C NMR (151 MHz, DMSO-d_6) δ 169.5, 169.3, 167.6, 167.4, 165.1, 165.0, 153.4, 150.7, 150.5, 147.4, 147.1, 141.0, 140.7, 139.3, 138.8, 134.5, 134.4, 133.4, 133.2, 132.0, 131.8, 129.7, 128.3, 128.1, 127.9, 127.8, 127.23, 127.16, 126.9, 126.8, 126.1, 125.6, 124.1, 123.8, 123.6, 123.4, 79.7, 53.4, 51.3, 49.1, 48.2, 42.3, 42.1, 28.0. HRMS (ESI) [M + H]$^+$: 594.2708, calcd for $C_{34}H_{36}N_5O_5$: 594.2711.

*tert-Butyl-{3-[4-({N-[2-(benzylamino)-2-oxoethyl]-3,5-dimethylbenzamido}methyl)benzamido]-[1,1′-biphenyl]-4-yl}-carbamate (**13d**).* White solid; 65%; mp 199 °C; t_R = 20.30 min, 98.0 purity; ^{1}H NMR (600 MHz, DMSO-d_6) δ 9.93 (s, 1H), 8.78 (s, 1H), 8.46*/8.42 (t, J = 5.6 Hz, 1H), 7.99−7.03 (m, 20H), 4.75/4.62* (s, 2H), 4.34*/4.29 (d, J = 5.6 Hz, 2H), 4.02*/3.82 (s, 2H), 2.25 (s, 6H), 1.47 (s, 9H). ^{13}C NMR (151 MHz, DMSO-d_6) δ 171.62, 171.61, 167.8, 167.7, 165.3, 165.1, 153.4, 141.4, 141.1, 139.3, 139.1, 137.6, 136.0, 135.9, 133.3, 133.2, 131.20, 131.15, 130.9, 130.8, 129.9, 129.0, 128.31, 128.27, 128.1, 127.9, 127.8, 127.4, 127.3, 127.2, 127.0, 126.9, 126.8, 126.4, 124.12, 124.08, 123.8, 79.8, 53.2, 51.1, 48.7, 47.6, 42.2, 42.1, 28.0, 20.8. HRMS (ESI) [M + H]$^+$: 697.3380, calcd for $C_{43}H_{45}N_4O_5$: 697.3384.

*tert-Butyl-{3-[4-({N-[2-(benzylamino)-2-oxoethyl]-4-(dimethylamino)benzamido}methyl)benzamido]-[1,1′-biphenyl]-4-yl}carbamate (**13e**).* Rose solid; 65%; mp 203 °C; ^{1}H NMR (600 MHz, DMSO-d_6) δ 9.93 (s, 1H), 8.77 (s, 1H), 8.52−8.43 (m, 1H), 7.99−6.66 (m, 21H), 4.74 (bs, 2H), 4.32 (d, J = 5.8 Hz, 2H), 3.93 (bs, 2H), 2.94 (s, 6H), 1.47 (s, 9H,). ^{13}C NMR (151 MHz, DMSO-d_6) δ 171.8, 168.2, 165.3, 153.4, 151.3, 141.7, 139.3, 135.8, 133.1, 131.2, 129.9, 129.0, 128.6, 128.3, 128.0, 127.9, 127.4, 127.3, 126.9, 126.4, 124.12, 124.05, 123.8, 111.0, 79.8, 42.1, 28.1. HRMS (ESI) [M + H]$^+$: 712.3490, calcd for $C_{43}H_{46}N_5O_5$: 712.3493. Anal calcd for $C_{43}H_{45}N_5O_5$: C 72.55, H 6.37, N 9.84; found: C 72.28, H 6.40, N 9.71.

*tert-Butyl-{2-[4-({N-[2-(benzylamino)-2-oxoethyl]-3,5-dimethylbenzamido}methyl)benzamido]-4-fluorophenyl}-carbamate (**13f**).* White solid; 65%; mp 191 °C; ^{1}H NMR (600 MHz, DMSO-d_6) δ 9.82 (s, 1H), 8.79 (bs, 1H), 8.46*/8.41 (t, J = 5.7 Hz, 1H), 7.95−7.03 (m, 15H), 4.74/4.61* (s, 2H), 4.33*/4.28 (d, J = 5.6 Hz, 2H), 4.01*/3.81 (s, 2H), 2.25 (s, 6H, 2 × H_3), 1.45 (s, 9H). ^{13}C NMR (151 MHz, DMSO-d_6) δ 171.6, 167.8, 167.6, 165.1, 164.9, 159.2, 157.6, 153.7, 141.6, 141.3, 139.3, 139.1, 137.6, 136.0, 135.8, 133.1, 133.0, 131.8, 131.8, 130.9, 130.9, 128.31, 128.27, 128.0, 127.9, 127.34, 127.25, 127.2, 127.1, 126.9, 126.8, 125.9, 124.1, 112.0, 111.9, 111.8, 111.7, 111.6, 79.7, 53.2, 51.1, 48.7, 47.6, 42.2, 42.1, 28.0, 20.8. HRMS (ESI) [M + H]$^+$: 639.2979, calcd for $C_{37}H_{40}FN_4O_5$: 639.2977. Anal calcd for $C_{37}H_{39}FN_4O_5$: C 69.58, H 6.15, N 8.77; found: C 69.81, H 6.21, N 8.78.

Biological Evaluation. *Reagents.* Cisplatin was purchased from Sigma (Germany) and dissolved in 0.9% sodium chloride solution, and propidium iodide (PI) was purchased from PromoKine

DOI: 10.1021/acs.jmedchem.9b01489
J. Med. Chem. 2019, 62, 11260−11279

(Germany). Vorinostat was synthesized according to known procedures.[30] Stock solutions (10 mM) of **1h**, **2a**, **2d**, entinostat, nexturastat A, and vorinostat were prepared with DMSO and diluted to the desired concentrations with the appropriate medium. All other reagents were supplied by PAN Biotech (Germany) unless otherwise stated.

Cell Lines and Cell Culture. The human ovarian carcinoma cell line A2780 was obtained from European Collection of Cell Cultures (ECACC, UK). The human tongue cell line Cal27 was obtained from the German Collection of Microorganisms and Cell Cultures (DSMZ, Germany). The corresponding cisplatin resistant CisR cell line Cal27CisR was generated by exposing the parental cell line to weekly cycles of cisplatin in an IC_{50} concentration over a period of 24−30 weeks as described in the studies of Gosepath et al. and Eckstein et al.[15,31] All cell lines were grown at 37 °C under humidified air supplemented with 5% CO_2 in RPMI 1640 (A2780) or DMEM (Cal27) containing 10% fetal calf serum, 120 IU/mL penicillin, and 120 μg/mL streptomycin. The cells were grown to 80% confluency before being used in further assays.

MTT Cell Viability Assay. The rate of cell-survival under the action of test substances was evaluated by an improved MTT assay as previously described.[32,33] A2780 and Cal27 cell lines were seeded at a density of 5000 and 2500 cells/well in 96 well plates (Corning, Germany). After 24 h, cells were exposed to increased concentrations of the test compounds. Incubation was ended after 72 h, and cell survival was determined by addition of MTT (Serva, Germany) solution (5 mg/mL in phosphate-buffered saline). The formazan precipitate was dissolved in DMSO (VWR, Germany). Absorbance was measured at 544 and 690 nm in a FLUOstar microplate reader (BMG LabTech, Germany). To investigate the effect of **1h**, **2a**, and **2d** on cisplatin-induced cytotoxicity, compounds were added 48 h before cisplatin administration. After 72 h, the cytotoxic effect was determined by the MTT assay as described above, and shift factors were calculated by dividing the IC_{50} value of cisplatin alone by the IC_{50} value of the drug combinations.

Combination Index Analysis. The combined effect of cisplatin and **1 h**, **2a**, or **2d** was analyzed using the MTT assay. Cell viability was determined from each well relative to the average absorbance of control wells. The combination indexes (CIs) were calculated with the CalcuSyn 2.1 software (BioSoft, Cambridge) based on the Chou−Talalay method. A CI > 1 indicates antagonism, a CI = 1 indicates an additive effect, and a CI < 1 indicates synergism.

Whole-Cell HDAC Inhibition Assay. The cellular HDAC assay was based on an assay published by Ciossek et al.[34] and Bonfils et al.[35] with minor modifications as described by Marek et al.[32]

Briefly, human cancer cell lines Cal27 and A2780 were seeded in 96-well tissue culture plates (Corning, Germany) at a density of 1.5×10^4 cells/well in a total volume of 90 μL of culture medium. After 24 h, cells were incubated for 18 h with increasing concentrations of test compounds. The reaction was started by adding 10 μL of 3 mM Boc-Lys(ε-Ac)-AMC (Bachem, Germany) to reach a final concentration of 0.3 mM.[36] Cells were incubated with Boc-Lys(ε-Ac)-AMC for 3 h under cell culture conditions. Then, 100 μL/well stop solution (25 mM Tris−HCl (pH 8), 137 mM NaCl, 2.7 mM KCl, 1 mM $MgCl_2$, 1% NP40, 2.0 mg/mL trypsin, 10 μM vorinostat) was added and the reaction was developed for 3 h under cell culture conditions. Fluorescence intensity was measured at an excitation of 320 nm and emission of 520 nm in a NOVOstar microplate reader (BMG LabTech, Offenburg, Germany).

Measurement of Apoptotic Nuclei. Cal27 and Cal27CisR cells were seeded at a density of 3×10^4 cells/well in 24-well plates (Sarstedt, Germany). Cells were treated with **1h**, **2a**, or **2d** and cisplatin alone or in combination for the indicated time points. The supernatant was removed after a centrifugation step, and the cells were lysed in 500 μL of hypotonic lysis buffer (0.1% sodium citrate, 0.1% Triton X-100, 100 μg/mL PI) at 4 °C in the dark overnight. The percentage of apoptotic nuclei with DNA content in sub-G1 was analyzed by flow cytometry using a CyFlow instrument (Partec, Germany).

Caspase 3/7 Activation Assay. Compound-induced activation of caspases 3 and 7 was analyzed using the CellEvent Caspase-3/7 green detection reagent (Thermo Scientific, Germany) according to the manufacturer's instructions. Briefly, Cal27 and Cal27CisR cells were seeded in 96-well-plates (Corning, Germany) at a density of 900 cells/well. Cells were treated with **1h**, **2a**, or **2d** 48 h prior to the addition of cisplatin and another incubation period of 24 h. Then, the medium was removed and 50 μL of the CellEvent Caspase 3/7 green detection reagent (2 μM in PBS supplemented with 5% heat-inactivated FBS) was added. Cells were incubated for 30 min at 37 °C in a humidified incubator before imaging by using the Thermo Fisher ArrayScan XTI high content screening (HCS) system (Thermo Scientific). Hoechst 33342 was used for nuclear staining. The pan caspase inhibitor QVD was used in a concentration of 20 μM diluted in the appropriate medium and incubated 30 min prior to compound addition.

Immunoblotting. Cells were treated with 5 μM **1h**, 0.5 μM **2a**, 3.2 μM **2d**, or the vehicle for 24 h. HDACi entinostat, nexturastat A, and vorinostat were used as controls. Cell pellets were dissolved with a RIPA buffer (50 mM Tris−HCl pH 8.0, 1% Triton X-100, 0.5% sodium deoxycholate, 0.1% SDS, 150 mM sodium chloride, 2 mM EDTA, supplemented with protease and phosphatase inhibitors (Pierce protease and phosphatase inhibitor mini tablets, Thermo Scientific)) and clarified by centrifugation. Equal amounts of total protein (20 μg) were resolved by SDS-PAGE and transferred to poly(vinylidene fluoride) membranes (Merck Millipore). Blots were incubated with primary antibodies against acetylated α-tubulin, α-tubulin (Santa Cruz Biotechnology, Germany), and acetyl histone H3 (Lys24) (Bio-Techne, Germany). Immunoreactive proteins were visualized using a luminol reagent (Santa Cruz Biotechnology, Germany) with an Intas Imager (Intas, Germany). Densitometric analysis was performed on scanned images using the Image J software (National Institutes of Health).[37]

Data Analysis. Concentration−effect curves were constructed with Prism 7.0 (GraphPad, San Diego, CA) by fitting the pooled data of at least three experiments performed in triplicate to the four-parameter logistic equation. Statistical analysis was performed using the *t* test or one-way ANOVA.

In Vitro HDAC1 and HDAC6 Assay. OptiPlate-96 black microplates (Perkin Elmer) were used with an assay volume of 50 μL. Human recombinant HDAC1 (10 ng/well; BPS Bioscience, catalog no.: 50051) or HDAC6 (35 ng/well; BPS Bioscience, catalog no.: 50006) were diluted in the assay buffer (50 mM Tris−HCl, pH 8.0, 137 mM NaCl, 2.7 mM KCl, 1 mM $MgCl_2$, 0.1 mg/mL BSA) followed by addition of different concentrations of test compounds or controls diluted in the assay buffer and 5 μL of the fluorogenic substrate ZMAL (Z-(Ac)Lys-AMC)[38] (150 μM) at 37 °C. After 90 min of incubation at 37 °C, 50 μL of 0.4 mg/mL trypsin in a trypsin buffer (Tris−HCl 50 mM, pH 8.0, NaCl 100 mM) was added followed by further incubation at 37 °C for 30 min. Fluorescence was measured with an excitation wavelength of 390 nm and an emission wavelength of 460 nm using a Spark 10M microplate reader (Tecan).

In Vitro HDAC2 and HDAC3 Assay. Black 96-well flat-bottom microplates (Corning Costar, Corning Inc., NY) were used. Human recombinant C-terminal FLAG-tag HDAC2 (BPS Bioscience, catalog no.: 50052) or human recombinant C-terminal His-tag HDAC3/NcoR2 (BPS Bioscience, catalog no.: 50003) was diluted in an incubation buffer (25 mM Tris−HCl, pH 8.0, 137 mM NaCl, 2.7 mM KCl, 1 mM MgCl, 0.01% Triton-X, 1 mg/mL BSA). This diluted solution (40 μL) was incubated with 10 μL of inhibitors with different concentrations in 10% DMSO/incubation buffer and 50 μL of fluorogenic Boc-Lys(ε-Ac)-AMC (20 μM, Bachem, Germany) at 37 °C. After 90 min incubation time, 50 μL of the stop solution (25 mM Tris−HCl (pH 8), 137 mM NaCl, 2.7 mM KCl, 1 mM $MgCl_2$, 0.01% Triton-X, 6.0 mg/mL trypsin from porcine pancreas Type IX-S, lyophilized powder, 13,000−20,000 BAEE units/mg protein (Sigma Aldrich), 200 μM vorinostat) was added. After a following incubation at 37 °C for 30 min, the fluorescence was measured on a Synergy H1 Hybrid Multi-Mode Microplate Reader (BioTek, USA) with a gain of

DOI: 10.1021/acs.jmedchem.9b01489
J. Med. Chem. 2019, 62, 11260−11279

70, an excitation wavelength of 370 nm, and an emission wavelength of 460 nm.

In Vitro HDAC4 and HDAC8 Assay. All human recombinant enzymes were purchased from Reaction Biology Corp. (Malvern, PA, USA). The HDAC activity assay of HDAC4 (catalog no. KDA-21-279) and HDAC8 (catalog no. KDA-21−481) was performed in 96-well plates (Corning, Germany). Briefly, 20 ng of HDAC8 and 2 ng of HDAC4 per reaction were used. Recombinant enzymes were diluted in the assay buffer (50 mM Tris−HCl, pH 8.0, 137 mM NaCl, 2.7 mM KCl, 1 mM $MgCl_2$, 1 mg/mL BSA). This diluted solution (80 μL) was incubated with 10 μL of inhibitors with different concentrations in the assay buffer. After a 5 min incubation step, the reaction was started with 10 μL of 100 μM (HDAC4) or 60 μM (HDAC8) Boc-Lys(TFa)-AMC (Bachem, Germany). The reaction was stopped after 90 min by adding 100 μL of stop solution (16 mg/mL trypsin, 2 μM panobinostat for HDAC8, 2 μM or CHDI0039 (kindly provided by the CHDI Foundation Inc., New York, USA) for HDAC4 in 50 mM Tris−HCl, pH 8.0, 100 mM NaCl. Fifteen minutes after the addition of the stop solution, the fluorescence intensity was measured at an excitation of 355 nm and emission of 460 nm in a NOVOstar microplate reader (BMG LabTech, Offenburg, Germany).

Docking Studies. We docked the *cis*- and *trans*-rotamers of compounds **1f**, **1h**, and **2a** into X-ray crystal structures of HDACs 1 (PDB ID: 4BKX),[39] 2 (PDB ID: 4LY1),[40] 3 (PDB ID: 4A69),[41] and 6 (PDB ID: 5EDU)[42] to understand and explain their selectivity profiles. All HDAC crystal structures were energy-minimized with Moloc using the MAB force field.[43] The compounds were drawn with ChemDraw Ultra, converted into a 3D structure, and energy-minimized with Moloc using the MAB force field.[43] The HDACi's were then docked into the HDAC structures utilizing AutoDock3[44] as a docking engine and the DrugScore[45,46] distance-dependent pair-potentials as an objective function, as described in ref 47. In the docking, default parameters were used with the exception of the clustering RMSD cutoff, which was set to 2.0 Å, to consider the flexibly connected saturated and unsaturated carbon cycles. Docking solutions with more than 20% of all configurations in the largest cluster were considered sufficiently converged. The configuration in the largest cluster with the lowest docking energy and with a distance of <3 Å between the hydroxamic acid oxygen and the zinc ion in the binding pocket was used for further evaluation.

PAINS Analysis. We filtered all compounds for pan-assay interference compounds (PAINS) using the online filter http://zinc15.docking.org/patterns/home/.[48] No compound was flagged as PAINS.

■ ASSOCIATED CONTENT

Supporting Information

The Supporting Information is available free of charge at https://pubs.acs.org/doi/10.1021/acs.jmedchem.9b01489.

Supplementary Table and Figures, ^{1}H and ^{13}C NMR spectra, and HPLC chromatograms (PDF)

Molecular formula strings and some data (CSV)

Coordinate information of docked complex (PDB, PDB, PDB, PDB)

■ AUTHOR INFORMATION

Corresponding Authors

*E-mail: matthias.kassack@uni-duesseldorf.de. Phone: +49 211 81-14587 (M.U.K.).

*E-mail: finn.hansen@medizin.uni-leipzig.de. Phone: (+49) 341 97 36801. Fax: (+49) 341 97 36889 (F.K.H.).

ORCID

Thomas Kurz: 0000-0002-9474-4224

Holger Gohlke: 0000-0001-8613-1447

Frank J. Dekker: 0000-0001-7217-9300

Finn K. Hansen: 0000-0001-9765-5975

Author Contributions

#V.K. and A.H. contributed equally to this work.

Author Contributions

‡M.U.K. and F.K.H. share the senior authorship.

Notes

The authors declare no competing financial interest.

■ ACKNOWLEDGMENTS

The Deutsche Forschungsgemeinschaft (DFG) is acknowledged for funds used to purchase the UHR-TOF maXis 4G, Bruker Daltonics, Bremen HRMS instrument used in this research. We further acknowledge funding by the DFG for the Thermofisher Arrayscan XTI (Grant: INST 208/690-1 FUGG to MUK). Experimental support (HDAC enzyme assays) by Christian Schrenk is gratefully acknowledged. The Center for Structural Studies is funded by the Deutsche Forschungsgemeinschaft (DFG Grant number 417919780).

■ ABBREVIATIONS

CisR, cisplatin resistant subclone; DIC, diisopropylcarbodiimide; EDC·HCl, *N*-(3-dimethylaminopropyl)-*N*′-ethylcarbodiimide hydrochloride; DMAP, 4-(dimethylamino)pyridine; Et_3N, triethylamine; HAT, histone acetyltransferase; HDAC, histone deacetylase; HDACi, histone deacetylase inhibitor; HOAt, 1-hydroxy-7-azabenzotriazol; MTT, 3-(4,5-dimethylthiazol-2-yl)-2,5-diphenyltetrazolium bromide; MS, molecular sieve; RT, room temperature; U-4CR, ugi 4-component reaction; ZBG, zinc-binding group.

■ REFERENCES

(1) (a) Wagner, J. M.; Hackanson, B.; Lübbert, M.; Jung, M. Histone deacetylase (HDAC) inhibitors in recent clinical trials for cancer therapy. *Clin. Epigenet.* **2010**, *1*, 117−136. (b) Witt, O.; Deubzer, H. E.; Milde, T.; Oehme, I. HDAC family: what are the cancer relevant targets? *Cancer Lett.* **2009**, *277*, 8−21. (c) Biel, M.; Wascholowski, V.; Giannis, A. Epigenetics - an epicenter of gene regulation: histones and histone-modifying enzymes. *Angew. Chem. Int. Ed.* **2005**, *44*, 3186−3216.

(2) New, M.; Olzscha, H.; La Thangue, N. B. HDAC inhibitor-based therapies: can we interpret the code? *Mol. Oncol.* **2012**, *6*, 637−656.

(3) Mottamal, M.; Zheng, S.; Huang, T.; Wang, G. Histone deacetylase inhibitors in clinical studies as templates for new anticancer agents. *Molecules* **2015**, *20*, 3898−3941.

(4) (a) Paris, M.; Porcelloni, M.; Binaschi, M.; Fattori, D. Histone deacetylase inhibitors: from bench to clinic. *J. Med. Chem.* **2008**, *51*, 1505−1529. (b) Andrews, K. T.; Haque, A.; Jones, M. K. HDAC inhibitors in parasitic diseases. *Immunol. Cell Biol.* **2012**, *90*, 66−77. (c) Xiao, H.; Jiao, J.; Wang, L.; O'Brien, S.; Newick, K.; Wang, L.-C. S.; Falkensammer, E.; Liu, Y.; Han, R.; Kapoor, V.; Hansen, F. K.; Kurz, T.; Hancock, W. W.; Beier, U. H. HDAC5 controls the functions of Foxp3$^+$ T-regulatory and CD8$^+$ T cells. *Int. J. Cancer* **2016**, *138*, 2477−2486. (d) Archin, N. M.; Liberty, A. L.; Kashuba, A. D.; Choudhary, S. K.; Kuruc, J. D.; Crooks, A. M.; Parker, D. C.; Anderson, E. M.; Kearney, M. F.; Strain, M. C.; Richman, D. D.; Hudgens, M. G.; Bosch, R. J.; Coffin, J. M.; Eron, J. J.; Hazuda, D. J.; Margolis, D. M. Administration of vorinostat disrupts HIV-1 latency in patients on antiretroviral therapy. *Nature* **2012**, *487*, 482−485. (e) Cao, F.; Zwinderman, M. R. H.; Dekker, F. J. The process and strategy for developing selective histone deacetylase 3 inhibitors. *Molecules* **2018**, *23*, 551. (f) Trazzi, S.; Fuchs, C.; Viggiano, R.; de Franceschi, M.; Valli, E.; Jedynak, P.; Hansen, F. K.; Perini, G.; Rimondini, R.; Kurz, T.; Bartesaghi, R.; Ciani, E. HDAC4: a key factor underlying brain developmental alterations in CDKL5 disorder. *Hum. Mol. Genet.* **2016**, *25*, 3887−3907. (g) Falkenberg, K. J.;

DOI: 10.1021/acs.jmedchem.9b01489
J. Med. Chem. 2019, 62, 11260−11279

Johnstone, R. W. Histone deacetylases and their inhibitors in cancer, neurological diseases and immune disorders. *Nat. Rev. Drug Discov.* **2014**, *13*, 673−691.
(5) Whittle, J. R.; Desai, J. Histone deacetylase inhibitors in cancer: what have we learned? *Cancer* **2015**, *121*, 1164−1167.
(6) Shen, S.; Kozikowski, A. P. Why hydroxamates may not be the best histone deacetylase inhibitors-what some may have forgotten or would rather forget? *ChemMedChem* **2016**, *11*, 15−21.
(7) Bressi, J. C.; Jennings, A. J.; Skene, R.; Wu, Y.; Melkus, R.; De Jong, R.; O'Connell, S.; Grimshaw, C. E.; Navre, M.; Gangloff, A. R. Exploration of the HDAC2 foot pocket: synthesis and SAR of substituted N-(2-aminophenyl)benzamides. *Bioorg. Med. Chem. Lett.* **2010**, *20*, 3142−3145.
(8) (a) Shi, Y.; Dong, M.; Hong, X.; Zhang, W.; Feng, J.; Zhu, J.; Yu, L.; Ke, X.; Huang, H.; Shen, Z.; Fan, Y.; Li, W.; Zhao, X.; Qi, J.; Zhou, D.; Ning, Z.; Lu, X. Results from a multicenter, open-label, pivotal phase II study of chidamide in relapsed or refractory peripheral T-cell lymphoma. *Ann. Oncol.* **2015**, 1766−1771. (b) Pan, D.-S.; Yang, Q.-J.; Fu, X.; Shan, S.; Zhu, J.-Z.; Zhang, K.; Li, Z.-B.; Ning, Z.-Q.; Lu, X.-P. Discovery of an orally active subtype-selective HDAC inhibitor, chidamide, as an epigenetic modulator for cancer treatment. *Med. Chem. Commun.* **2014**, *5*, 1789−1796.
(9) (a) Roche, J.; Bertrand, P. Inside HDACs with more selective HDAC inhibitors. *Eur. J. Med. Chem.* **2016**, *121*, 451−483. (b) Rai, M.; Soragni, E.; Chou, C. J.; Barnes, G.; Jones, S.; Rusche, J. R.; Gottesfeld, J. M.; Pandolfo, M. Two new pimelic diphenylamide HDAC inhibitors induce sustained frataxin upregulation in cells from Friedreich's ataxia patients and in a mouse model. *PLoS One* **2010**, *5*, No. e8825.
(10) (a) Diedrich, D.; Hamacher, A.; Gertzen, C. G. W.; Alves Avelar, L. A.; Reiss, G. J.; Kurz, T.; Gohlke, H.; Kassack, M. U.; Hansen, F. K. Rational design and diversity-oriented synthesis of peptoid-based selective HDAC6 inhibitors. *Chem. Commun.* **2016**, *52*, 3219−3222. (b) Porter, N. J.; Osko, J. D.; Diedrich, D.; Kurz, T.; Hooker, J. M.; Hansen, F. K.; Christianson, D. W. Histone deacetylase 6-selective inhibitors and the influence of capping groups on hydroxamate-zinc denticity. *J. Med. Chem.* **2018**, *61*, 8054−8060. (c) Diedrich, D.; Stenzel, K.; Hesping, E.; Antonova-Koch, Y.; Gebru, T.; Duffy, S.; Fisher, G.; Schöler, A.; Meister, S.; Kurz, T.; Avery, V. M.; Winzeler, E. A.; Held, J.; Andrews, K. T.; Hansen, F. K. One-pot, multi-component synthesis and structure-activity relationships of peptoid-based histone deacetylase (HDAC) inhibitors targeting malaria parasites. *Eur. J. Med. Chem.* **2018**, *158*, 801−813.
(11) Krieger, V.; Hamacher, A.; Gertzen, C. G. W.; Senger, J.; Zwinderman, M. R. H.; Marek, M.; Romier, C.; Dekker, F. J.; Kurz, T.; Jung, M.; Gohlke, H.; Kassack, M. U.; Hansen, F. K. Design, multicomponent synthesis, and anticancer activity of a focused histone deacetylase (HDAC) inhibitor library with peptoid-based cap groups. *J. Med. Chem.* **2017**, *60*, 5493−5506.
(12) Kim, R.; Skolnick, J. Assessment of programs for ligand binding affinity prediction. *J. Comput. Chem.* **2008**, *29*, 1316−1331.
(13) Jurkin, J.; Zupkovitz, G.; Lagger, S.; Grausenburger, R.; Hagelkruys, A.; Kenner, L.; Seiser, C. Distinct and redundant functions of histone deacetylases HDAC1 and HDAC2 in proliferation and tumorigenesis. *Cell Cycle* **2011**, *10*, 406−412.
(14) Bradner, J. E.; Hnisz, D.; Young, R. A. Transcriptional addiction in cancer. *Cell* **2017**, *168*, 629−643.
(15) Gosepath, E. M.; Eckstein, N.; Hamacher, A.; Servan, K.; von Jonquieres, G.; Lage, H.; Györffy, B.; Royer, H. D.; Kassack, M. U. Acquired cisplatin resistance in the head-neck cancer cell line Cal27 is associated with decreased DKK1 expression and can partially be reversed by overexpression of DKK1. *Int. J. Cancer* **2008**, *123*, 2013−2019.
(16) Chou, T.-C. Drug combination studies and their synergy quantification using the Chou-Talalay method. *Cancer Res.* **2010**, *70*, 440−446.
(17) Piro, G.; Roca, M. S.; Bruzzese, F.; Carbone, C.; Iannelli, F.; Leone, A.; Volpe, M. G.; Budillon, A.; Di Gennaro, E. Vorinostat potentiates 5-fluorouracil/cisplatin combination by inhibiting chemotherapy-induced EGFR nuclear translocation and increasing cisplatin uptake. *Mol. Cancer Ther.* **2019**, *18*, 1405−1417.
(18) Chen, S.-H.; Chang, J.-Y. New insights into mechanisms of cisplatin resistance: from tumor cell to microenvironment. *Int. J. Mol. Sci.* **2019**, *20*, 4136.
(19) Autin, P.; Blanquart, C.; Fradin, D. Epigenetic drugs for cancer and microRNAs: a focus on histone deacetylase inhibitors. *Cancers* **2019**, *11*, 1530.
(20) Pchejetski, D.; Alfraidi, A.; Sacco, K.; Alshaker, H.; Muhammad, A.; Monzon, L. Histone deacetylases as new therapy targets for platinum-resistant epithelial ovarian cancer. *J. Cancer Res Clin. Oncol.* **2016**, *142*, 1659−1671.
(21) Bandolik, J. J.; Hamacher, A.; Schrenk, C.; Weishaupt, R.; Kassack, M. U. Class I-histone deacetylase (HDAC) inhibition is superior to pan-HDAC inhibition in modulating cisplatin potency in high grade serous ovarian cancer cell lines. *Int. J. Mol. Sci.* **2019**, *20*, 3052.
(22) Stenzel, K.; Hamacher, A.; Hansen, F. K.; Gertzen, C. G. W.; Senger, J.; Marquardt, V.; Marek, L.; Marek, M.; Romier, C.; Remke, M.; Jung, M.; Gohlke, H.; Kassack, M. U.; Kurz, T. Alkoxyurea-based histone deacetylase inhibitors increase cisplatin potency in chemoresistant cancer cell lines. *J. Med. Chem.* **2017**, *60*, 5334−5348.
(23) Jakobsen, C. M.; Denmeade, S. R.; Isaacs, J. T.; Gady, A.; Olsen, C. E.; Christensen, S. B. Design, synthesis, and pharmacological evaluation of thapsigargin analogues for targeting apoptosis to prostatic cancer cells. *J. Med. Chem.* **2001**, *44*, 4696−4703.
(24) Grosse, S.; Pillard, C.; Himbert, F.; Massip, S.; Léger, J. M.; Jarry, C.; Bernard, P.; Guillaumet, G. Access to imidazo[1,2-*a*]imidazolin-2-ones and functionalization through Suzuki−Miyaura cross-coupling reactions. *Eur. J. Org. Chem.* **2013**, *2013*, 4146−4155.
(25) West, C. W.; Estiarte, M. A.; Rich, D. H. New methods for side-chain protection of cysteine. *Org. Lett.* **2001**, *3*, 1205−1208.
(26) Reynolds, D.; Hao, M.-H.; Wang, J.; Prajapati, S.; Satoh, T.; Selvaraj, A. Pyrimidine FGFR4 Inhibitors. International Patent WO2015/57938A1 April 23, 2015.
(27) Dallavalle, S.; Cincinelli, R.; Nannei, R.; Merlini, L.; Morini, G.; Penco, S.; Pisano, C.; Vesci, L.; Barbarino, M.; Zuco, V.; De Cesare, M.; Zunino, F. Design, synthesis, and evaluation of biphenyl-4-yl-acrylohydroxamic acid derivatives as histone deacetylase (HDAC) inhibitors. *Eur. J. Med. Chem.* **2009**, *44*, 1900−1912.
(28) Rusche, J. R.; Peet, N. P.; Hoppoer, A. T. Compositions including 6-Aminohexanoic Acid Derivatives as HDAC Inhibitors. U.S. Patent 9,265,734 April 19, 2012.
(29) Mazitschek, R.; Ghosh, B.; Hendricks, J. A.; Reis, S.; Haggarty, S. J. Photoswitchable HDAC Inhibitors. International Patent WO2014/160221A1 October 2, 2014.
(30) Gediya, L. K.; Chopra, P.; Purushottamachar, P.; Maheshwari, N.; Njar, V. C. O. A new simple and high-yield synthesis of suberoylanilide hydroxamic acid and its inhibitory effect alone or in combination with retinoids on proliferation of human prostate cancer cells. *J. Med. Chem.* **2005**, *48*, 5047−5051.
(31) Eckstein, N.; Servan, K.; Girard, L.; Cai, D.; von Jonquieres, G.; Jaehde, U.; Kassack, M. U.; Gazdar, A. F.; Minna, J. D.; Royer, H. D. Epidermal growth factor receptor pathway analysis identifies amphiregulin as a key factor for cisplatin resistance of human breast cancer cells. *J. Biol. Chem.* **2008**, *283*, 739−750.
(32) Marek, L.; Hamacher, A.; Hansen, F. K.; Kuna, K.; Gohlke, H.; Kassack, M. U.; Kurz, T. Histone deacetylase (HDAC) inhibitors with a novel connecting unit linker region reveal a selectivity profile for HDAC4 and HDAC5 with improved activity against chemoresistant cancer cells. *J. Med. Chem.* **2013**, *56*, 427−436.
(33) Engelke, L. H.; Hamacher, A.; Proksch, P.; Kassack, M. U. Ellagic acid and resveratrol prevent the development of cisplatin resistance in the epithelial ovarian cancer cell line A2780. *J. Cancer.* **2016**, *7*, 353−363.
(34) Ciossek, T.; Julius, H.; Wieland, H.; Maier, T.; Beckers, T. A homogeneous cellular histone deacetylase assay suitable for compound profiling and robotic screening. *Anal. Biochem.* **2008**, *372*, 72−81.

DOI: 10.1021/acs.jmedchem.9b01489
J. Med. Chem. 2019, 62, 11260−11279

(35) Bonfils, C.; Kalita, A.; Dubay, M.; Siu, L. L.; Carducci, M. A.; Reid, G.; Martell, R. E.; Besterman, J. M.; Li, Z. Evaluation of the pharmacodynamic effects of MGCD0103 from preclinical models to human using a novel HDAC enzyme assay. *Clin. Cancer Res.* **2008**, *14*, 3441−3449.
(36) Hoffmann, K.; Jung, M.; Brosch, G.; Loidl, P. A Non-isotopic assay for histone deacetylase activity. *Nucl. Acids Res.* **1999**, *27*, 2057−2058.
(37) Schneider, C. A.; Rasband, W. S.; Eliceiri, K. W. NIH image to ImageJ: 25 years of image analysis. *Nat. Methods* **2012**, *9*, 671−675.
(38) Heltweg, B.; Dequiedt, F.; Verdin, E.; Jung, M. Nonisotopic substrate for assaying both human zinc and NAD+-dependent histone deacetylases. *Anal. Biochem.* **2003**, *319*, 42−48.
(39) Millard, C. J.; Watson, P. J.; Celardo, I.; Gordiyenko, Y.; Cowley, S. M.; Robinson, C. V.; Fairall, L.; Schwabe, J. W. R. Class I HDACs share a common mechanism of regulation by inositol phosphates. *Mol. Cell* **2013**, *51*, 57−67.
(40) Lauffer, B. E. L.; Mintzer, R.; Fong, R.; Mukund, S.; Tam, C.; Zilberleyb, I.; Flicke, B.; Ritscher, A.; Fedorowicz, G.; Vallero, R.; Ortwine, D. F.; Gunzner, J.; Modrusan, Z.; Neumann, L.; Koth, C. M.; Lupardus, P. J.; Kaminker, J. S.; Heise, C. E.; Steiner, P. Histone deacetylase (HDAC) inhibitor kinetic rate constants correlate with cellular histone acetylation but not transcription and cell viability. *J. Biol. Chem.* **2013**, *288*, 26926−26943.
(41) Watson, P. J.; Fairall, L.; Santos, G. M.; Schwabe, J. W. R. Structure of HDAC3 bound to co-repressor and inositol tetraphosphate. *Nature* **2012**, *481*, 335−340.
(42) Hai, Y.; Christianson, D. W. Histone deacetylase 6 structure and molecular basis of catalysis and inhibition. *Nat. Chem. Biol.* **2016**, *12*, 741−747.
(43) Gerber, P. R.; Müller, K. MAB, a generally applicable molecular force field for structure modelling in medicinal chemistry. *J. Comput.-Aided Mol. Des.* **1995**, *9*, 251−268.
(44) Goodsell, D. S.; Morris, G. M.; Olson, A. J. Automated docking of flexible ligands: application of Autodock. *J. Mol. Recognit.* **1996**, *9*, 1−5.
(45) Gohlke, H.; Hendlich, M.; Klebe, G. Knowledge-based scoring function to predict protein-ligand interactions. *J. Mol. Biol.* **2000**, *295*, 337−356.
(46) Dittrich, J.; Schmidt, D.; Pfleger, C.; Gohlke, H. Converging a knowledge-based scoring function: DrugScore^{2018}. *J. Chem. Inf. Model.* **2019**, *59*, 509−521.
(47) Sotriffer, C. A.; Gohlke, H.; Klebe, G. Docking into knowledge-based potential fields: a comparative evaluation of DrugScore. *J. Med. Chem.* **2002**, *45*, 1967−1970.
(48) Baell, J. B.; Holloway, G. A. New substructure filters for removal of pan assay interference compounds (PAINS) from screening libraries and for their exclusion in bioassays. *J. Med. Chem.* **2010**, *53*, 2719−2740.

DOI: 10.1021/acs.jmedchem.9b01489
J. Med. Chem. 2019, 62, 11260−11279